iScience

CellPress
OPEN ACCESS

Article

PABPC1 mediates degradation of *C9orf72*-FTLD/ALS GGGGCC repeat RNA

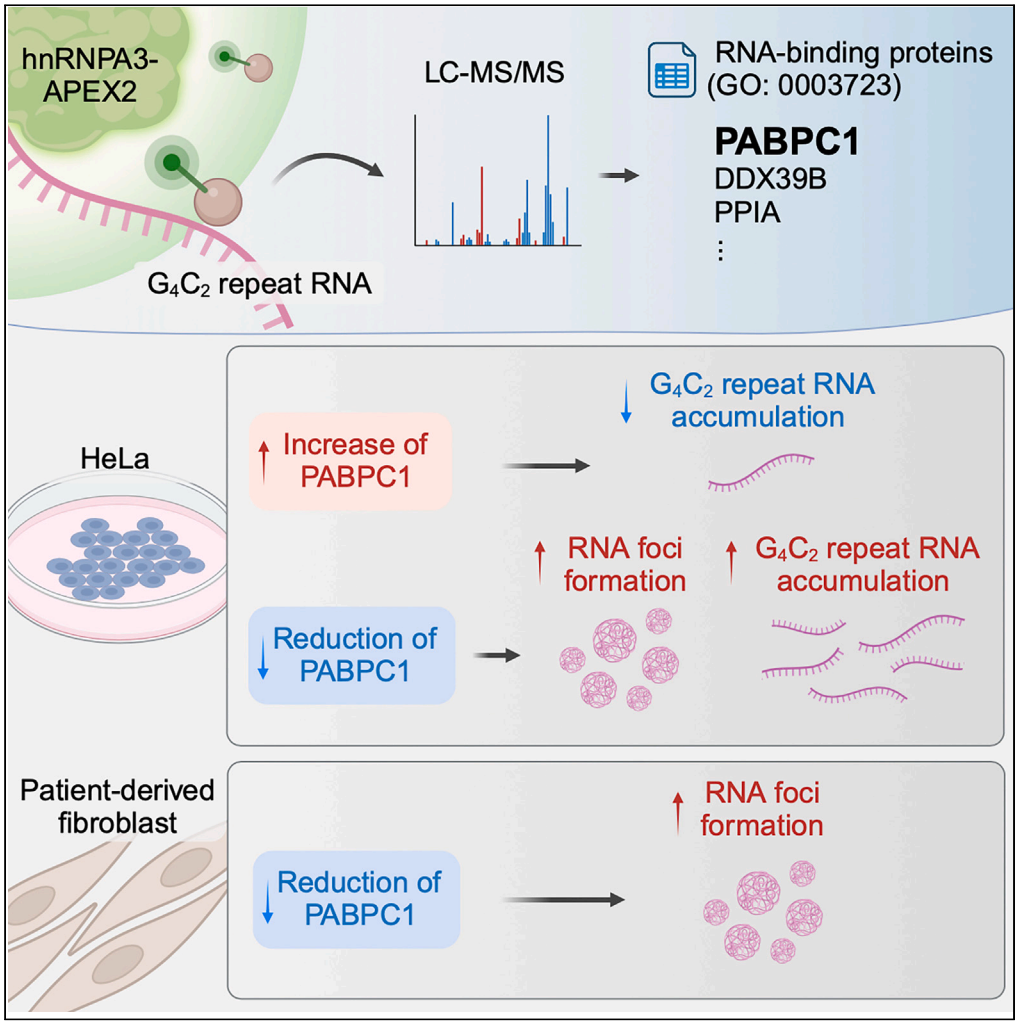

Ryota Uozumi, Kohji Mori, Shiho Gotoh, ..., Shinji Tagami, Shoshin Akamine, Manabu Ikeda

kmori@psy.med.osaka-u.ac.jp

Highlights

APEX2 proximity labeling combined with LC-MS identified interactors of hnRNPA3

Reduction of PABPC1 increases RNA foci in patient-derived fibroblasts

PABPC1 and hnRNPA3 cooperate in the degradation of *C9orf72* G_4C_2 repeat RNA

PABPC1 interacts with RNA exosome complex in the presence of G_4C_2 repeat RNA

Uozumi et al., iScience *27*, 109303
March 15, 2024
https://doi.org/10.1016/j.isci.2024.109303

iScience

CellPress
OPEN ACCESS

Article

PABPC1 mediates degradation of *C9orf72*-FTLD/ALS GGGGCC repeat RNA

Ryota Uozumi,[1] Kohji Mori,[1,4,*] Shiho Gotoh,[1] Tesshin Miyamoto,[1] Shizuko Kondo,[1] Tomoko Yamashita,[1] Yuya Kawabe,[1,2] Shinji Tagami,[2,3] Shoshin Akamine,[1] and Manabu Ikeda[1]

SUMMARY

GGGGCC hexanucleotide repeat expansion in *C9orf72* causes frontotemporal lobar degeneration and amyotrophic lateral sclerosis. Expanded GGGGCC repeat RNA accumulates within RNA foci and is translated into toxic dipeptide repeat proteins; thus, efficient repeat RNA degradation may alleviate diseases. hnRNPA3, one of the repeat RNA-binding proteins, has been implicated in the destabilization of repeat RNA. Using APEX2-mediated proximity biotinylation, here, we demonstrate PABPC1, a cytoplasmic poly (A)-binding protein, interacts with hnRNPA3. Knockdown of PABPC1 increased the accumulation of repeat RNA and RNA foci to the same extent as the knockdown of hnRNPA3. Proximity ligation assays indicated PABPC1-hnRNPA3 and PABPC1-RNA exosomes, a complex that degrades repeat RNA, preferentially co-localized when repeat RNA was present. Our results suggest that PABPC1 functions as a mediator of polyadenylated GGGGCC repeat RNA degradation through interactions with hnRNPA3 and RNA exosome complex.

INTRODUCTION

Frontotemporal lobar degeneration (FTLD) and amyotrophic lateral sclerosis (ALS) are seemingly distinct but pathologically and genetically overlapping neurodegenerative diseases.[1,2] Hexanucleotide repeat expansion in the non-coding region of the *C9orf72* gene is the most common genetic mutation that causes familial forms of both FTLD and ALS (*C9*-FTLD/ALS).[3] The expanded DNA repeat region is transcribed in both the sense and antisense directions and produces GGGGCC (G_4C_2) or CCCCGG (C_4G_2) repeat-containing RNA (repeat RNA). The accumulated repeat RNA forms RNA foci, which may selectively sequester a subset of RNA-binding proteins (RBPs), thereby impairing the physiological functions of these RBPs. G_4C_2 and C_4G_2 repeat RNAs can even be translated in all possible reading frames into dipeptide repeat proteins (DPR) termed poly-GA, poly-GR, poly-PR, poly-PA, and poly-GP (from sense and antisense strands) through repeat-associated non-AUG (RAN) translation.[4,5] Pathologically, DPR co-localizes with the selective autophagy adaptor p62, most prominently in the hippocampus and cerebellum in the postmortem brains of *C9*-FTLD/ALS patients.[4–7] Repeat RNA foci are also predominantly found in neuronal nuclei in the hippocampus, cerebellum, frontal, and motor cortices,[8–11] and rarely in microglia, astrocytes, and oligodendrocytes.[8,9] Since the repeat RNA is positioned upstream of the pathological disease cascade, promoting its degradation is a way to overcome neurodegeneration; however, the underlying mechanism of repeat RNA degradation is still largely unclear.

Heterogeneous nuclear ribonucleoprotein A3 (hnRNPA3) has been identified as an RBP that selectively binds to G_4C_2 repeat RNA.[12] hnRNPA3 co-localizes with a portion of DPR inclusions in the hippocampal dentate gyrus of patients, implying that it is closely involved in the pathogenesis of *C9*-FTLD/ALS.[13–16] hnRNPA3 is involved in RNA splicing, mRNA stabilization, and translation.[17] Structurally, hnRNPA3 is characterized by two RNA recognition motifs at the N-terminus and a glycine-rich low-complexity (LC) domain at the C-terminus.[13] Such structures are highly common among RBPs,[18] and hnRNPA3 itself is not thought to have the enzymatic activity to degrade RNA. We previously reported that decreased expression of hnRNPA3 led to the accumulation of G_4C_2 repeat RNA in cells derived from *C9orf72* mutation carriers and corresponding DPRs in cellular models of *C9*-FTLD/ALS.[15,16] Interestingly, overexpression of wild-type hnRNPA3 reduced poly-GA expression, but RNA-binding ability deficient mutant hnRNPA3 overexpression failed to suppress DPR expression levels in the cellular model or the *Drosophila* model.[15,19] From these observations, we hypothesized that hnRNPA3 that binds to G_4C_2 repeat RNA may physically interact with RNA degradation factors and facilitate selective RNA degradation in cells.

Several hnRNPs, including hnRNPA3, have been reported to undergo liquid-liquid phase separation (LLPS) in cells to form membrane-less organelles.[18,20] LLPS is a complex process that partially involves the LC domains of these RBPs, which tend to enhance weak intermolecular interactions, including electrostatic and π–π interactions.[21,22] *In vitro* and in cells, RBPs incorporate RNA or single-stranded DNA into

[1]Department of Psychiatry, Graduate School of Medicine, Osaka University, Suita, Osaka 565-0871, Japan
[2]Psychiatry, Minoh Neuropsychiatric Hospital, Minoh, Osaka 562-0004, Japan
[3]Health and Counseling Center, Osaka University, Toyonaka, Osaka 560-0043, Japan
[4]Lead contact
*Correspondence: kmori@psy.med.osaka-u.ac.jp
https://doi.org/10.1016/j.isci.2024.109303

phase-separated droplets.[20,21] These droplets may serve as sites for efficient RNA metabolism.[22,23] Hence, physiological weak interactions between hnRNPA3 and its proximal proteins may be essential for the repeat RNA degradation pathway in the cellular environment.

Immunoprecipitation is a useful approach to assessing intermolecular interactions, but its application is limited to analyzing molecules with high-affinity interactions.[24] This limitation may prevent the identification of proteins with relatively weak intermolecular interactions, such as those involved in LLPS. One way to overcome such limitations is to apply proximity-labeling technology. Ascorbate peroxidase (APEX) is generated from class I cytosolic plant peroxidase and developed as an alternative tag to gain high-resolution intracellular imaging using electron microscopy[25] and subsequently adapted for proximity labeling technology.[26] Recently, a mutated version of APEX, APEX2, was generated to improve the sensitivity of proximity-labeling reactions.[27] APEX2 is a 27 kDa peroxidase that converts biotin-phenol (BP) to biotin-phenoxyl radicals in the presence of hydrogen peroxide (H_2O_2) in living cells.[24,27,28] Oxidized BP is highly sensitive and short-lived (<1 ms)[29]; hence, the APEX2 assay enables specific biotinylation of cellular molecules that are proximal (<20 nm) to APEX2 active sites.[24,25,28,30] Biotinylated proteins are easily purified using streptavidin beads and can be identified using liquid chromatography-tandem mass spectrometry (LC-MS/MS).

In this study, to elucidate the G_4C_2 repeat RNA degradation pathway involving hnRNPA3, an APEX2 proximity-labeling proteomics assay was performed using hnRNPA3 fused to APEX2 to comprehensively identify proteins in the proximity of hnRNPA3 in living cells.

RESULTS

Proximity biotin-phenol labeling by hnRNPA3-APEX2 in HeLa cells

hnRNPA3 is potentially involved in the G_4C_2 repeat RNA degradation pathway. However, no intrinsic RNase activity has so far been reported,[17] and structurally, it is not assumed to have RNase activity. Therefore, we hypothesized that hnRNPA3 might interact with genuine RNA-degrading proteins. To comprehensively identify proteins close to hnRNPA3 in living cells, we performed the APEX2 proximity labeling assay (Figure 1A).[24,26] First, V5-tagged APEX2 was fused to the C-terminal glycine-rich LC domain through which hnRNPA3 interacts with other proteins (Figure 1B).[13,20] We then expressed the hnRNPA3-V5-APEX2 construct in HeLa cells under the control of the CMV promoter. Western blot analysis confirmed hnRNPA3-V5-APEX2 protein expression at the expected molecular weight (Figure 1C). hnRNPA3 is a nucleocytoplasmic shuttling protein with nuclear predominance under physiological conditions. Consistent with this, immunofluorescence analysis confirmed that hnRNPA3-V5-APEX2 was localized mainly to the nucleus, with a weak cytoplasmic distribution (Figure 1D). Next, to assess the biotinylation activity of hnRNPA3-V5-APEX2, transfected cells were stimulated with BP and H_2O_2 for up to 30 min (Figure 1E). Biotinylated proteins in whole-cell lysates were then visualized using SDS-PAGE with a streptavidin-HRP conjugate. This time-course analysis revealed that APEX2-mediated biotinylation occurred within 1 min of incubation and that further accumulation of biotinylated proteins was observed in time-dependent manner (Figures 1F, 1G, and S1). The specificity of APEX2-dependent biotinylation was supported by the observation that biotinylated signals were very subtle in the absence of either the hnRNPA3-V5-APEX2 construct, BP, or H_2O_2. Some biotinylated proteins found in non-stimulated conditions can be explained by endogenous biotinylated proteins, such as enzyme-biotin intermediates of carboxylase reactions that use biotin as a co-factor.[31] To avoid excessive biotinylation, which may lead to nonspecific biotin labeling, we applied 1-min stimulation in the following experiments. While hnRNPA3-V5-APEX2 was localized mainly to the nucleus and weakly to the cytoplasm as a shuttling hnRNP (Figure 1D), immunofluorescence with NeutrAvidin-Alexa Fluor 488 revealed that biotinylation was relatively enriched in the cytoplasm of these cells (Figure 1H). This could be due to the limited access of BP through the nuclear membrane.[32] These results confirmed that hnRNPA3-V5-APEX2 exhibits biotin-labeling activity in living cells and preferentially labels cytoplasmic proteins. Since cytoplasmic G_4C_2 repeat RNA can be an immediate substrate for RAN translation and hnRNPA3 may suppress DPR expression by promoting G_4C_2 repeat RNA degradation, we focused on the analysis of the cytoplasm-enriched factors coupled with hnRNPA3-mediated G_4C_2 repeat RNA degradation, which can be approached with this system.

APEX2 proteomics for identification of proximity proteins of hnRNPA3

To identify proximal interactors of hnRNPA3 that may be involved in G_4C_2 repeat RNA degradation, we performed APEX2 assay in the presence or absence of $(G_4C_2)_{80}$ repeat-expression, followed by identification with LC-MS/MS (Figures 2A and 2B). To begin, we confirmed that poly-GA was produced through RAN translation in repeat expressing HeLa cells, as previously reported (Figure 2C).[15,33] Cells co-expressing $(G_4C_2)_{80}$ and hnRNPA3-V5-APEX2 were treated with BP and H_2O_2 to biotinylate intracellular factors in the proximity of hnRNPA3-V5-APEX2. After cell lysis, biotinylated proteins were pulled down using streptavidin magnetic beads. The samples were then dialyzed and separated using SDS-PAGE. Detection with streptavidin-HRP revealed that biotinylated proteins were selectively increased in cells treated with BP (Figure 2D). Each sample was subjected to LC-MS/MS analysis to identify these biotinylated proteins quantitatively and qualitatively (Figure 2E). We identified a total of 552 proteins (Figure 2F, and Table S1). The following filtering protocol was then applied to prioritize the proteins that might be involved in the degradation of the *C9orf72* G_4C_2 repeat RNA (Figure 2F). First, 190 proteins that were detected more than twice out of three by LC-MS/MS were selected. Among these, 66 proteins were selected for which the absolute differences between the expression and non-expression of $(G_4C_2)_{80}$ in average quantitative value (AQV) were equal to or more than 2.00 (Figure 2F). We initially intended to identify hnRNPA3-related RNA-degrading factors (e.g., RNases); however, apparent RNA-degrading proteins were not included in the list of these 66 proteins. Second, to gain more insight into their functions, Gene Ontology analysis (GO analysis) was performed (Figures 2G and 2H), and we focused on 24 RNA binding proteins (GO: 0003723) that were significantly enriched and presumed to be most relevant for RNA-degrading activity. Among the 24 proteins, we excluded 15 hnRNP family proteins from further analysis because they also have no direct RNA-degrading activities predicted from their structures similar to hnRNPA3. Through APEX proteomics and subsequent filtering, we selected nine RNA binding proteins (SFPQ, ALYREF, PPIA, DDX39B, FKBP4, DHX9, SF3B2, PABPC1, and DDX5), whose abundance varied with the presence or absence of the $(G_4C_2)_{80}$ repeat RNA, as potential factors that might be relevant to hnRNPA3 mediated G_4C_2 repeat RNA degradation (Figures 2F–2H, Tables S1, and S2).

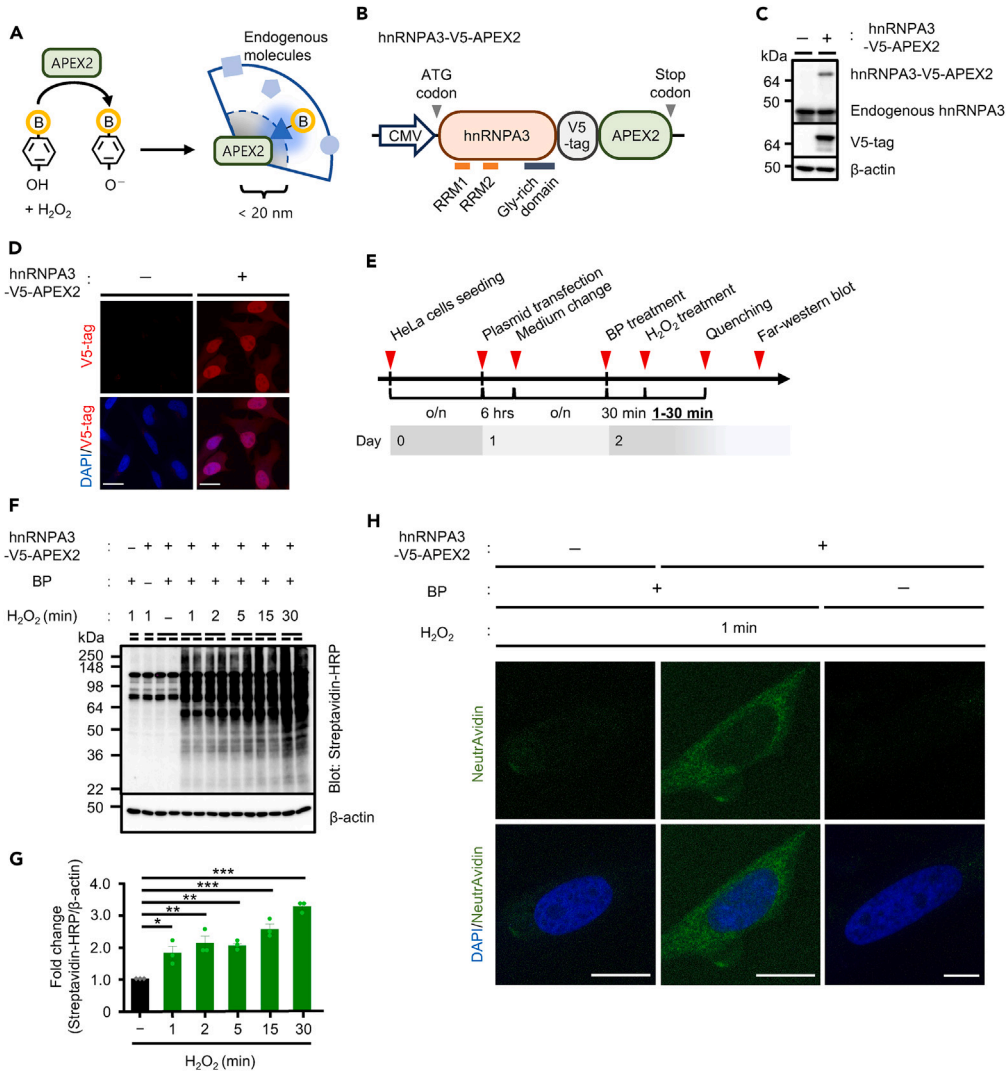

Figure 1. Biotin-phenol (BP)-labeling activity of hnRNPA3-V5-APEX2 protein in HeLa cells

(A) Schematic of APEX2 proximity labeling assay.

(B) Schema showing the construct expressing the hnRNPA3-APEX2 fusion protein with inserted V5 tag.

(C) Detection of hnRNPA3-V5-APEX2 expression by western blotting with an anti-hnRNPA3, an anti-V5 tag, and anti-β-actin antibodies.

(D) Fluorescence images of HeLa cells expressing hnRNPA3-V5-APEX2 with an anti-V5 tag antibody. Nuclei were visualized with DAPI.

(E) Timeline outlining the time-course assay to verify the BP labeling of hnRNPA3-V5-APEX2. The starting point (Day 0) was the seeding of HeLa cells.

(F) Representative image of the time-course assay of hnRNPA3-V5-APEX2 biotinylation. The construct was expressed in HeLa cells and treated with BP/H_2O_2 (for 1, 2, 5, 15, and 30 min) detected by the streptavidin-HRP conjugate.

(G) Quantification of the hnRNPA3-V5-APEX2 biotinylation time-course assay. Three independent experiments were performed.

(H) Spatial characterization of hnRNPA3-V5-APEX2-mediated biotinylation. Biotinylated molecules were visualized using the NeutrAvidin-Alexa Fluor 488 (AF488) conjugate. Nuclei were visualized with DAPI. Scale bars = 20 μm. RRM, RNA recognition motif; Gly, glycine. *$p < 0.05$, **$p < 0.001$, and ***$p < 0.0001$ by one-way ANOVA with Dunnett's multiple-comparison test to non-H_2O_2 treatment (–). A circle in the graphs represents the mean of two biological replicates. See also Figure S1.

Identification of proteins associated with *C9orf72* repeat RNA degradation

To test whether these nine RBPs indeed affect G_4C_2 repeat RNA degradation, a secondary siRNA screening using quantitative reverse transcription (qRT)-PCR was performed on G_4C_2 repeat RNA-expressing HeLa cells. Interestingly, of the nine RBP candidates, G_4C_2 repeat RNA accumulation increased only when PABPC1 expression was reduced with the corresponding siRNA (Figure 3A). Conversely, siRNA-mediated knockdown of PPIA, FKBP4, and DDX39B reduced repeat RNA accumulation while DDX39B reduction missed statistical significance ($p = 0.076$). Reductions of the other five RBPs did not affect the repeat RNA accumulation compared to non-targeting control knockdown (Figure 3A). These results implicate that four of the nine RBPs we have identified as potential hnRNPA3 interactors affect the G_4C_2 repeat RNA metabolism.

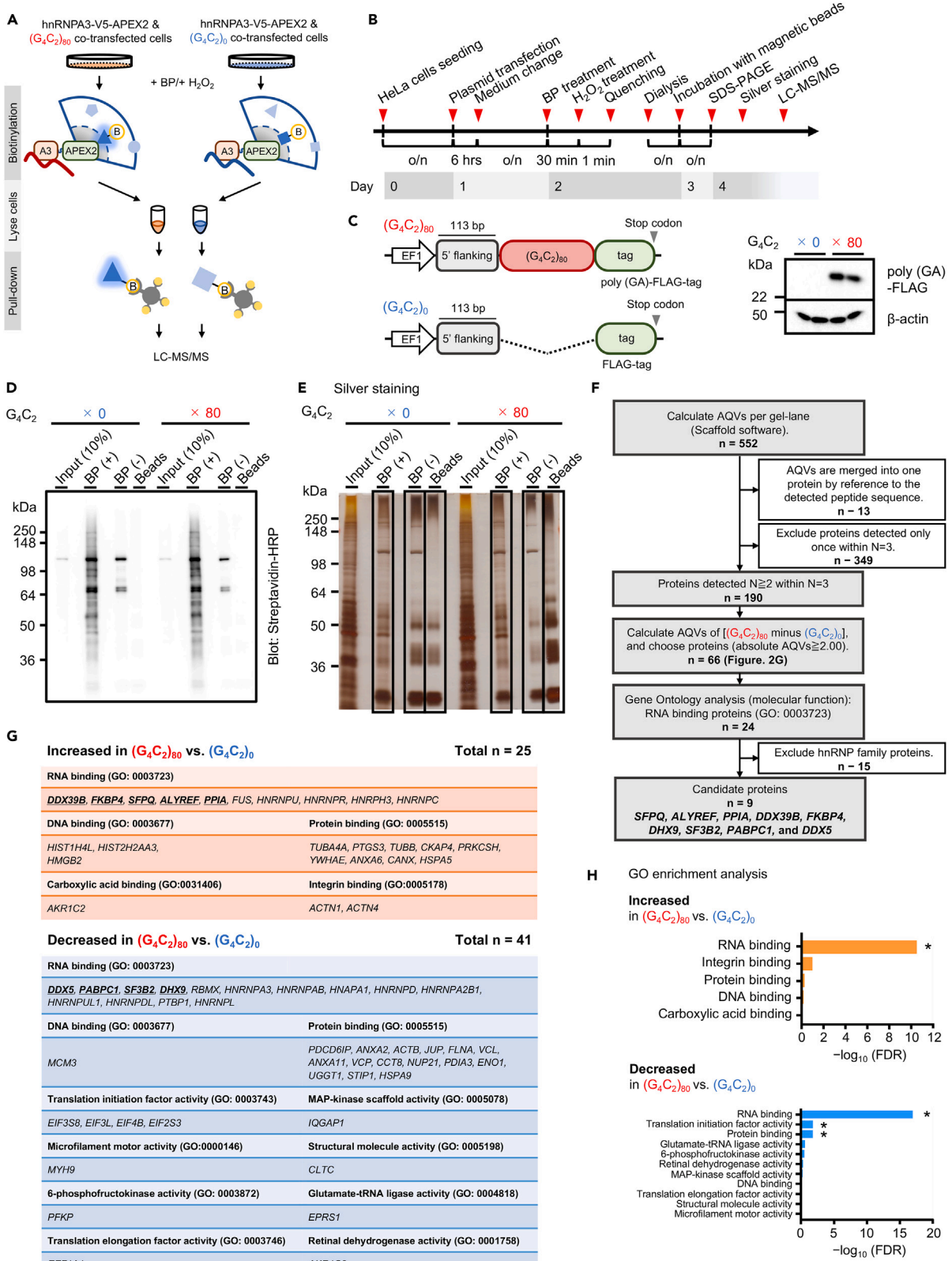

G

Increased in $(G_4C_2)_{80}$ vs. $(G_4C_2)_0$ — **Total n = 25**

RNA binding (GO: 0003723)	
***DDX39B*, *FKBP4*, *SFPQ*, *ALYREF*, *PPIA*, FUS, HNRNPU, HNRNPR, HNRPH3, HNRNPC**	
DNA binding (GO: 0003677)	**Protein binding (GO: 0005515)**
HIST1H4L, HIST2H2AA3, HMGB2	*TUBA4A, PTGS3, TUBB, CKAP4, PRKCSH, YWHAE, ANXA6, CANX, HSPA5*
Carboxylic acid binding (GO:0031406)	**Integrin binding (GO:0005178)**
AKR1C2	*ACTN1, ACTN4*

Decreased in $(G_4C_2)_{80}$ vs. $(G_4C_2)_0$ — **Total n = 41**

RNA binding (GO: 0003723)	
***DDX5*, *PABPC1*, *SF3B2*, *DHX9*, RBMX, HNRNPA3, HNRNPAB, HNAPA1, HNRNPD, HNRNPA2B1, HNRNPUL1, HNRNPDL, PTBP1, HNRNPL**	
DNA binding (GO: 0003677)	**Protein binding (GO: 0005515)**
MCM3	*PDCD6IP, ANXA2, ACTB, JUP, FLNA, VCL, ANXA11, VCP, CCT8, NUP21, PDIA3, ENO1, UGGT1, STIP1, HSPA9*
Translation initiation factor activity (GO: 0003743)	**MAP-kinase scaffold activity (GO: 0005078)**
EIF3S8, EIF3L, EIF4B, EIF2S3	*IQGAP1*
Microfilament motor activity (GO:0000146)	**Structural molecule activity (GO: 0005198)**
MYH9	*CLTC*
6-phosphofructokinase activity (GO: 0003872)	**Glutamate-tRNA ligase activity (GO: 0004818)**
PFKP	*EPRS1*
Translation elongation factor activity (GO: 0003746)	**Retinal dehydrogenase activity (GO: 0001758)**
EEF1A1	*AKR1C3*

Figure 2. Screening for identification of proximity proteins of hnRNPA3-APEX2 using LC-MS/MS and Gene Ontology (GO) analysis

(A) Schematic of APEX2 proteomics.

(B) Timeline of APEX2 proteomics with seeding of HeLa cells as the starting point (Day 0).

(C) Schematic representation of plasmids expressing $(G_4C_2)_{80}$ repeats and $(G_4C_2)_0$ repeats. Both constructs contained an FLAG tag. Each plasmid was expressed in HeLa cells and detected by western blotting with an anti-FLAG-tag antibody.

(D and E) hnRNPA3-V5-APEX2 expressing HeLa cells were treated with BP/H_2O_2 and pulled down using streptavidin magnetic beads. (D) Detection of biotin signals using streptavidin-HRP conjugate. (E) Silver staining (n = 3). Black boxes indicate the lanes in which LC-MS/MS analysis were performed.

(F) Flowchart of the filtering of candidate proteins potentially involved in G_4C_2 repeat RNA degradation from the 552 proteins identified by LC-MS/MS. QVs reflected the signal intensity calculated by the Scaffold software.

(G) List of genes encoding proteins for which the absolute difference in AQVs between $(G_4C_2)_{80}$ or $(G_4C_2)_0$ repeats was equal to or more than 2.00 in the LC-MS/MS analysis. Genes were classified using GO analysis. Nine RNA-binding proteins (RBPs) underlined were selected for secondary knockdown screening for G_4C_2 repeat RNA expression.

(H) GO enrichment analysis of 25 or 41 (increased or decreased in $[G_4C_2]_{80}$ vs. $[G_4C_2]_0$) proteins that screened with AVQs using PANTHER classification system. bp, base pair; BP (+), BP-treated; BP (−), BP-non-treated; Beads, streptavidin magnetic beads only; QV, quantitative value calculated in Scaffold software; AQV, average of QVs within n = 3; FDR, false discovery rate. An asterisk (*) indicates FDR $p < 0.05$. See also Table S1 andS2.

PPIA and DDX39B maintain *C9orf72* repeat RNA expression

In our secondary screening, we found that siRNA-mediated knockdown of PPIA, FKBP4, and DDX39B decreased repeat RNA accumulation (Figure 3A). To exclude the off-target effects of siRNA and confirm the target effects, we performed qRT-PCR using alternative siRNAs targeting different sequences of each RBP (Figure S2). As a result, we validated that the reduction of PPIA and DDX39B led to a decrease in the accumulation of repeat RNA in *C9orf72* repeat-expressing HeLa cells (Figure S2B and S2D). Therefore, in contrast to hnRNPA3 and PABPC1, PPIA and FKBP4 appear to maintain the expression levels of G_4C_2 repeat RNA via unidentified mechanisms. Although the mechanisms of action of these molecules are of interest, the primary aim of this study was to find a repeat RNA degradation pathway associated with hnRNPA3, and henceforth, the following analyses in this study focused on PABPC1, which may be involved in the degradation pathway.

Reduced PABPC1 expression promotes *C9orf72* repeat RNA accumulation

PABPC1, a cytoplasmic isoform of poly (A)-binding proteins (PABP), directly binds to the polyadenylated sites of both unspliced and fully spliced mRNA in mammalian cells.[34] Structurally, it contains four RNA recognition motifs (RRMs) in the N-terminal domain and one helical domain consisting of five α-helices in the C-terminal domain.[35] PABPC1 is localized in stress granules (SGs) during cellular stress conditions[36,37] and regulates RNA processes by incorporating mRNA into SGs.[22,38]

First, in addition to the original siRNA targeting PABPC1 used in the secondary screening (#5), the knockdown of PABPC1 with another siRNA targeting a different region (#7) confirmed the accumulation of repeat RNA in the $(G_4C_2)_{80}$-expressing HeLa cells, as observed in those cells upon hnRNPA3 knockdown (Figures 3B and 3C). Moreover, overexpression of siRNA-resistant PABPC1 reduced the accumulation of $(G_4C_2)_{80}$ repeat RNA, with or without knockdown of endogenous PABPC1 (Figures 3D and 3E), further validating the involvement of PABPC1 in G_4C_2 repeat RNA degradation. Next, we tested whether a reduction in PABPC1 promotes the formation of repeat RNA foci as a disease-associated phenotype of repeat RNA accumulation.[19,39] Fluorescence *in situ* hybridization (FISH) analysis of $(G_4C_2)_{80}$ expressing HeLa cells revealed that siRNA-mediated knockdown of PABPC1 increased the number of $(G_4C_2)_{80}$ repeat RNA foci positive cells, which is comparable to cells with hnRNPA3 knockdown (Figures 3F and 3G). These results suggest that PABPC1 is involved in the degradation pathway of G_4C_2 repeat RNA as well as hnRNPA3.

PABPC1 is involved in the degradation of *in vitro* transcribed *C9orf72* repeat RNA

To further validate the involvement of PABPC1 in the G_4C_2 repeat RNA degradation pathway, irrespective of transcription, we performed a time-dependent degradation assay of *in vitro* transcribed $(G_4C_2)_{80}$ repeat RNA in the cells. First, we synthesized *in vitro* both 5′ cap- and 3′ poly (A)-attached $(G_4C_2)_0$ or $(G_4C_2)_{80}$ repeat RNA using each plasmid DNA as a template (Figure 2C). Agarose-formamide gel electrophoresis confirmed expected RNA product sizes (Figure 3H). Next, *in vitro* transcribed G_4C_2 repeat RNA was transfected into PABPC1-knockdown HeLa cells and quantified its amount at each time point (0, 3, 6, and 12 h) by qRT-PCR (Figure 3I). As expected, we found that the stability of G_4C_2 repeat RNA was relatively maintained in PABPC1-knockdown cells compared with the control knockdown cells (Figure 3J). Our results support that PABPC1 is indeed involved in the degradation pathway of G_4C_2 repeat RNA.

PABPC1 and hnRNPA3 collaborate in the *C9orf72* repeat RNA degradation pathway

If PABPC1 and hnRNPA3 are in proximity, where does this occur in the cell? PABPC1 is enriched in the cytoplasm and partially shuttles into the nucleus.[35,40] hnRNPA3 also shuttles between the nucleus and cytoplasm but is predominantly located in the nucleus and partially in the cytoplasm under physiological conditions.[41] Immunostaining revealed that PABPC1 was prominently localized in the cytoplasm, regardless of hnRNPA3-V5-APEX2 expression (Figure S3).

To gain additional evidence of *in vivo* interaction between PABPC1 and hnRNPA3, together with information on localization, we performed fluorescence *in situ* proximity labeling assay (PLA). Close protein-protein interactions within approximately 40 nm produce a PLA signal through the hybridization of a pair of oligonucleotide-conjugated antibodies.[42,43] Strikingly, while the cells expressing $(G_4C_2)_0$ repeats showed weak PLA signals between the anti-PABPC1 and anti-hnRNPA3 antibodies, the cells expressing $(G_4C_2)_{80}$ repeat RNA showed

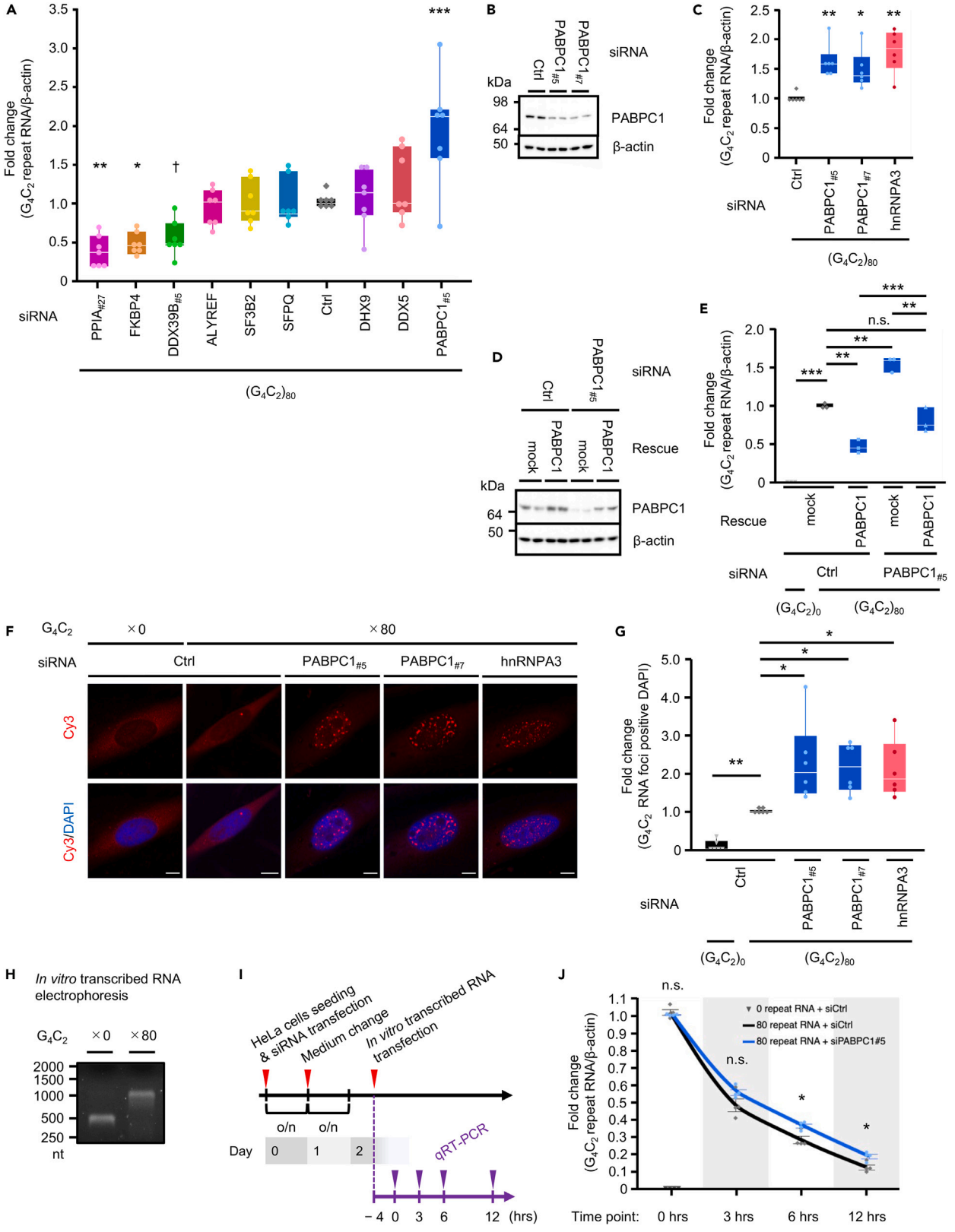
A
Fold change (G4C2 repeat RNA/β-actin)
siRNA
PPIA#27
FKBP4
DDX39B#5
ALYREF
SF3B2
SFPQ
Ctrl
DHX9
DDX5
PABPC1#5
(G4C2)80
B
siRNA
Ctrl
PABPC1#5
PABPC1#7
kDa
98
64
50
PABPC1
β-actin
C
Fold change (G4C2 repeat RNA/β-actin)
siRNA
Ctrl
PABPC1#5
PABPC1#7
hnRNPA3
(G4C2)80
D
siRNA
Ctrl
PABPC1#5
Rescue
mock
PABPC1
kDa
64
50
PABPC1
β-actin
E
Fold change (G4C2 repeat RNA/β-actin)
n.s.
Rescue
mock
PABPC1
siRNA
Ctrl
PABPC1#5
(G4C2)0
(G4C2)80
F
G4C2
×0
×80
siRNA
Ctrl
PABPC1#5
PABPC1#7
hnRNPA3
Cy3
Cy3/DAPI
G
Fold change (G4C2 RNA foci positive DAPI)
siRNA
Ctrl
PABPC1#5
PABPC1#7
hnRNPA3
(G4C2)0
(G4C2)80
H
In vitro transcribed RNA electrophoresis
G4C2
×0
×80
2000
1500
1000
500
250
nt
I
HeLa cells seeding & siRNA transfection
Medium change
In vitro transcribed RNA transfection
o/n
o/n
Day
0
1
2
qRT-PCR
−4
0
3
6
12
(hrs)
J
n.s.
0 repeat RNA + siCtrl
80 repeat RNA + siCtrl
80 repeat RNA + siPABPC1#5
n.s.
Fold change (G4C2 repeat RNA/β-actin)
Time point:
0 hrs
3 hrs
6 hrs
12 hrs

Figure 3. siRNA-mediated single knockdown screening identified G_4C_2 repeat RNA degrading-associated RNA-binding proteins (RBPs)

(A and C) Quantification of accumulated G_4C_2 repeat RNA was normalized to β-actin. Quantitative RT-PCR was performed in seven (A) or six (C) independent experiments.

(B) Western blotting images of the knockdown efficacy of two siRNAs targeting PABPC1.

(D) The expression of siRNA-resistant PABPC1 in HeLa cells was detected by western blotting with anti-PABPC1 and anti-β-actin antibodies.

(E) Quantification of accumulated G_4C_2 repeat RNA normalized to β-actin in rescue analysis. Quantitative RT-PCR was performed in three independent experiments.

(F and G) siRNA-mediated single knockdown of PABPC1 increased RNA foci in HeLa cells expressing $(G_4C_2)_{80}$ repeats, as visualized by FISH targeting sense repeat sequences. Six independent experiments were performed.

(H) Agarose-formaldehyde gel electrophoresis image of 5′ cap- and 3′ poly (A)-attached *in vitro* transcribed $(G_4C_2)_0$ or $(G_4C_2)_{80}$ repeat RNA. *In vitro* transcription of $(G_4C_2)_{80}$ repeat RNA was performed in four independent test tubes.

(I) Timeline of *in vitro* transcribed G_4C_2 repeat RNA degradation assay.

(J) Quantification of time-dependent degradation of G_4C_2 repeat RNA was normalized to β-actin. Quantitative RT-PCR was performed in four independent experiments. Quantification of $(G_4C_2)_0$ repeat RNA was only performed at 0 h time point. Scale bars = 10 μm. Ctrl, non-targeting siRNA; $PABPC1_{\#5}$ or $_{\#7}$, siRNA targeting PABPC1; $PPIA_{\#27}$, siRNA targeting PPIA; $DDX39B_{\#5}$, siRNA targeting DDX39B. *$p < 0.05$, **$p < 0.001$, ***$p < 0.0001$, and $^{\dagger}p = 0.076$. n.s.; not significant by one-way ANOVA with Dunnett's multiple-comparison test to control (A, C, and G), Tukey's HSD test (E), or two-tailed paired Student's *t*-test {([G_4C_2]$_{80}$ repeat RNA + siCtrl) vs. ([G_4C_2]$_{80}$ repeat RNA + siPABPC1$_{\#5}$)} (J). A circle in the graphs represents the mean of two biological replications (A, C, E, and J) or a result from the single culture well (G). The center lines in the boxplots represent the median, with the 25th and 75th percentiles marked by the box limits. The whiskers represent the farthest data points, and the circles outside the boxes are outliers. The line graphs represent the mean ± SEM. See also Figure S2 and S3.

increased PLA signals (Figures 4A and 4B). Negative control PLA staining using either the PABPC1 antibody or hnRNPA3 antibody showed few nonspecific signals, thus validating the specificity of the PLA signals (Figures 4A and 4B). Positive PLA signals were particularly enriched in the cytoplasm; however, some signals were also detected in the nucleus. This finding is consistent with the predominant cytoplasmic biotinylation observed in our APEX2 assay (Figure 1G).

Next, we investigated whether PABPC1 and hnRNPA3 are involved in the same pathway of G_4C_2 repeat RNA degradation. To do so, we performed qRT-PCR and FISH upon simultaneous knockdown of PABPC1 and hnRNPA3. If PABPC1 and hnRNPA3 function in the same RNA degradation pathway, no additive effect would be expected upon the double knockdown of these proteins, whereas if they are on distinct degradation pathways, then there should be an additive effect on G_4C_2 repeat RNA accumulation. As a result, two siRNA-mediated simultaneous knockdowns of both PABPC1 and hnRNPA3 did not show additive effects on the accumulation of G_4C_2 repeat RNA (Figure 4C), and formation of $(G_4C_2)_{80}$ repeat RNA foci (Figures 4D and 4E). Previously, increased expression of hnRNPA3 has induced G_4C_2 repeat RNA reduction in the cellular model or the *Drosophila* model.[15,19] Therefore, if PABPC1 is involved in the G_4C_2 repeat RNA degradation pathway in collaboration with hnRNPA3, PABPC1 reduction would diminish the effect of hnRNPA3 overexpression. Indeed, an increased expression of hnRNPA3 reduced $(G_4C_2)_{80}$ repeat RNA, and this effect was compromised by siRNA-mediated PABPC1 knockdown (Figure 4F). Together, these results suggest that PABPC1 and hnRNPA3 in proximity collaborate in the same pathway of G_4C_2 repeat RNA degradation.

Reduced PABPC1 expression promotes *C9orf72* repeat RNA foci formation in patient-derived cells

The expression of plasmid-derived G_4C_2 repeat RNA had artificial sequences, including linker and tag regions, and the other plasmid-derived sequences included a 3′ poly (A) tail. Since PABPC1 specifically binds to the poly (A) tail of mRNA, it is possible that APEX2 proteomics identified PABPC1 due to an artificial effect. Therefore, the crucial question is whether PABPC1 affects the degradation of G_4C_2 repeat RNA in an endogenous sequence context in cells derived from *C9*-FTLD/ALS patients. To answer this question, siRNA-mediated knockdown of PABPC1 was performed in fibroblasts from *C9*-FTLD/ALS patients and healthy controls,[33] and sense repeat RNA foci were visualized using FISH (Figure 5A, S4A, and S4D). Reductions in PABPC1 and hnRNPA3 increased both the frequency of G_4C_2 repeat RNA foci positive nuclei and the number of RNA foci per nucleus compared to those of control knockdown (Figures 5B, 5C, S4B, S4C, S4E, and S4F). These results indicate that PABPC1 is indeed involved and collaborates with hnRNPA3 in the RNA degradation pathway of disease-causing expanded G_4C_2 repeat RNA in *C9orf72* patient-derived cells.

PABPC1-mediated *C9orf72* repeat RNA degradation pathway

Structurally, PABPC1 itself, as well as hnRNPA3, were assumed to have no RNA degradation function. Our recent study reported that the RNA exosome complex is involved in G_4C_2 repeat RNA degradation.[33] Decreased expression levels of the RNA exosome complex, which consists of the core region and two ribonuclease subunits (EXOSC10 and DIS3), promote the accumulation of G_4C_2 repeat RNA and the formation of nuclear RNA foci in the cells.[33] Furthermore, PABPN1, one of the most abundant PABP isoforms in the nucleus, recognizes poly (A)-containing RNA and functions as an adaptor of the RNA exosome complex for RNA degradation.[44–46] Based on these findings, we hypothesized that PABPC1 interacts with the RNA exosome complex to effectively degrade G_4C_2 repeat RNA. EXOSC10 is known to be enriched in the nucleoli, but a weak cytoplasmic distribution of EXOSC10 is also recognized, and DIS3 is both in the nucleus and cytoplasm.[33,47] Thus, to investigate the interaction of PABPC1 and the RNA exosome complex in cells, we performed PLA in $(G_4C_2)_{80}$ repeat-expressing cells. $(G_4C_2)_{80}$ repeat-expressing HeLa cells showed more prominent PLA signals in the cytoplasm than $(G_4C_2)_0$ repeat-expressing cells, whereas the negative

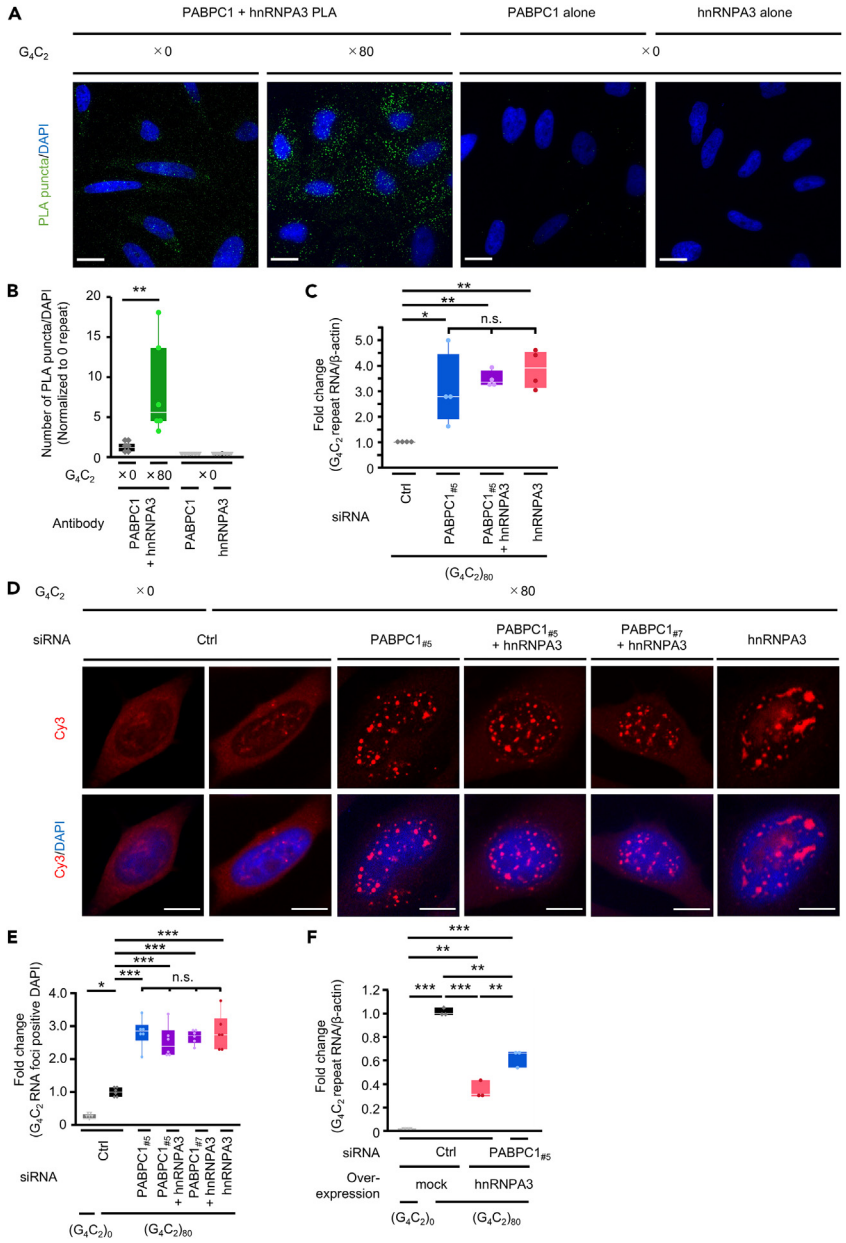

Figure 4. Single and double knockdown of PABPC1 and hnRNPA3 increased G_4C_2 repeat RNA accumulation and RNA foci formation to the same level

(A and B) The proximity labeling assay (PLA) signal intensity of PABPC1 and hnRNPA3 was increased in HeLa cells expressing the $(G_4C_2)_{80}$ repeat. Six independent experiments were performed.

(C) Relative quantification of accumulated G_4C_2 repeat RNA normalized to β-actin in siRNA-mediated double knockdown of PABPC1 and hnRNPA3. Four independent experiments were performed.

(D and E) siRNA-mediated double knockdown of PABPC1 and hnRNPA3 increased RNA foci in HeLa cells expressing the $(G_4C_2)_{80}$ repeat, as visualized by FISH targeting the sense repeat sequence.

(F) Quantification of accumulated G_4C_2 repeat RNA was normalized to β-actin. Quantitative RT-PCR was performed in three independent experiments. Scale bars = 20 μm (A) and 10 μm (D). Ctrl, non-targeting siRNA; $PABPC1_{\#5}$ or $_{\#7}$, siRNA targeting PABPC1. *$p < 0.05$, **$p < 0.001$, and ***$p < 0.0001$. n.s.; not significant by two-tailed paired Student's *t*-test (B) or one-way ANOVA with Tukey's HSD test (C, E, and F). A circle in the graphs represents the mean of two biological replications (C and F) or a result of a single culture well (B and E). The center lines in the boxplots represent the median, with the 25th and 75th percentiles marked by the box limits. The whiskers represent the farthest data points. See also Figure S3.

controls (PABPC1 alone, EXOSC10 alone, and DIS3 alone) showed few signals (Figures 6A–6D). In addition, when we reduced the expression of each protein using siRNA, we detected weaker PLA signals than control knockdown in $(G_4C_2)_{80}$ repeat-expressing cells (Figure S5). This indicates that these PLA signals were certainly derived from targeted protein-protein interactions. XRN1 is a major 5′→3′ exoribonuclease

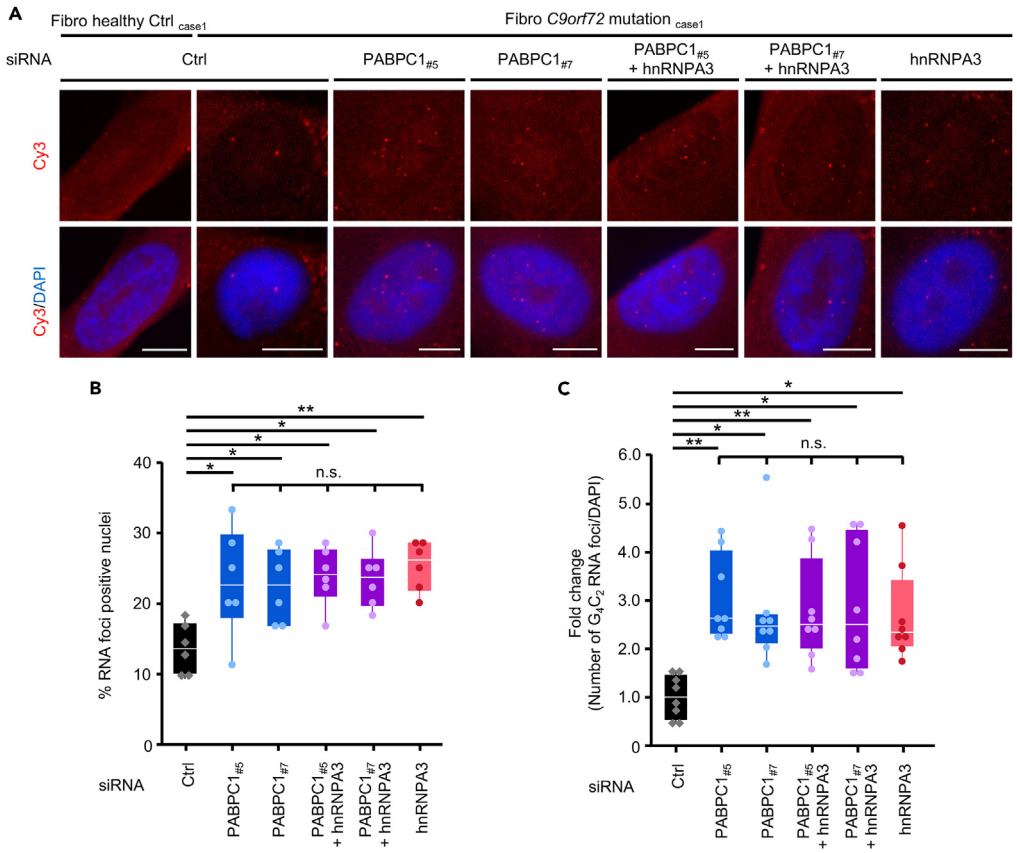

Figure 5. Knockdown of PABPC1 increased RNA foci formation in the *C9orf72* mutation carrier-derived cells

(A) siRNA-mediated single or double knockdown of PABPC1 and hnRNPA3 increased RNA foci in the *C9orf72* mutation carrier-derived fibroblasts visualized by FISH targeting the sense repeat sequence. Nuclei were stained with DAPI.

(B) Quantification of % RNA foci positive nuclei. Six independent experiments were performed.

(C) Quantification of the number of RNA foci/nuclei. Eight independent experiments were performed. Scale bars = 10 μm. Ctrl, non-targeting siRNA; PABPC1$_{\#5}$ or $_{\#7}$, siRNA targeting PABPC1. *$p < 0.05$, and **$p < 0.001$. n.s.; not significant by one-way ANOVA with Tukey's HSD test. A circle in the graphs represents a result of a single culture well. The center lines in the boxplots represent the median, with the 25th and 75th percentiles marked by the box limits. The whiskers represent the farthest data points, and the circles outside the boxes are outliers. See also Figure S4.

in the cytoplasm, degrading RNA in the opposite direction to the RNA exosome complex. If the RNA exosome complex and PABPC1 interact on the 3′ side of the RNA, XRN1, which is on the 5′ side of the RNA substrate, is not expected to be present in the proximity of PABPC1. To experimentally validate this expectation, PLA of PABPC1 and XRN1 was performed (Figures 6E and 6F). In clear contrast to the PLA of PABPC1 and the components of the RNA exosome complex (Figures 6A–6D), the PLA signals of PABPC1-XRN1 did not increase in $(G_4C_2)_{80}$ repeat-expressing cells (Figures 6E and 6F). This result further implicates the specific contribution of PABPC1 to RNA exosome-mediated G_4C_2 repeat RNA degradation. These results suggest that in the presence of G_4C_2 repeat RNA, PABPC1 is in proximity with the RNA exosome complex, a genuine and pervasive RNA-degrading machinery.

Differential effects of PABPC1 and hnRNPA3 on RAN translation

In eukaryotic cells, the 5′ cap and 3′ poly (A) tail of mRNA are structurally required for efficient translation. PABP interacts with translation initiation factors, such as eIF4G, to recognize the 5′ cap and form a closed-loop mRNA structure, which helps protein synthesis through efficient AUG-dependent translation.[40,48] To investigate the effect of PABPC1 or hnRNPA3 reduction on global translation, we performed a SUnSET assay.[49] Puromycin, an analog of aminoacyl-tRNA, was incorporated into the newly synthesized peptide chains. The signal intensity of puromycin-labeled proteins reflects the efficiency of global translation. Compared with the non-targeting control, PABPC1 and hnRNPA3 knockdown did not affect the amount of puromycin-incorporated protein (Figures S6A and S6B). When the cells were treated with cycloheximide (CHX), the signal intensity of puromycin was significantly reduced (Figures S6A and S6C). These results suggest that the transient reduction of PABPC1 and/or hnRNPA3 did not compromise global translation, at least under our experimental conditions.

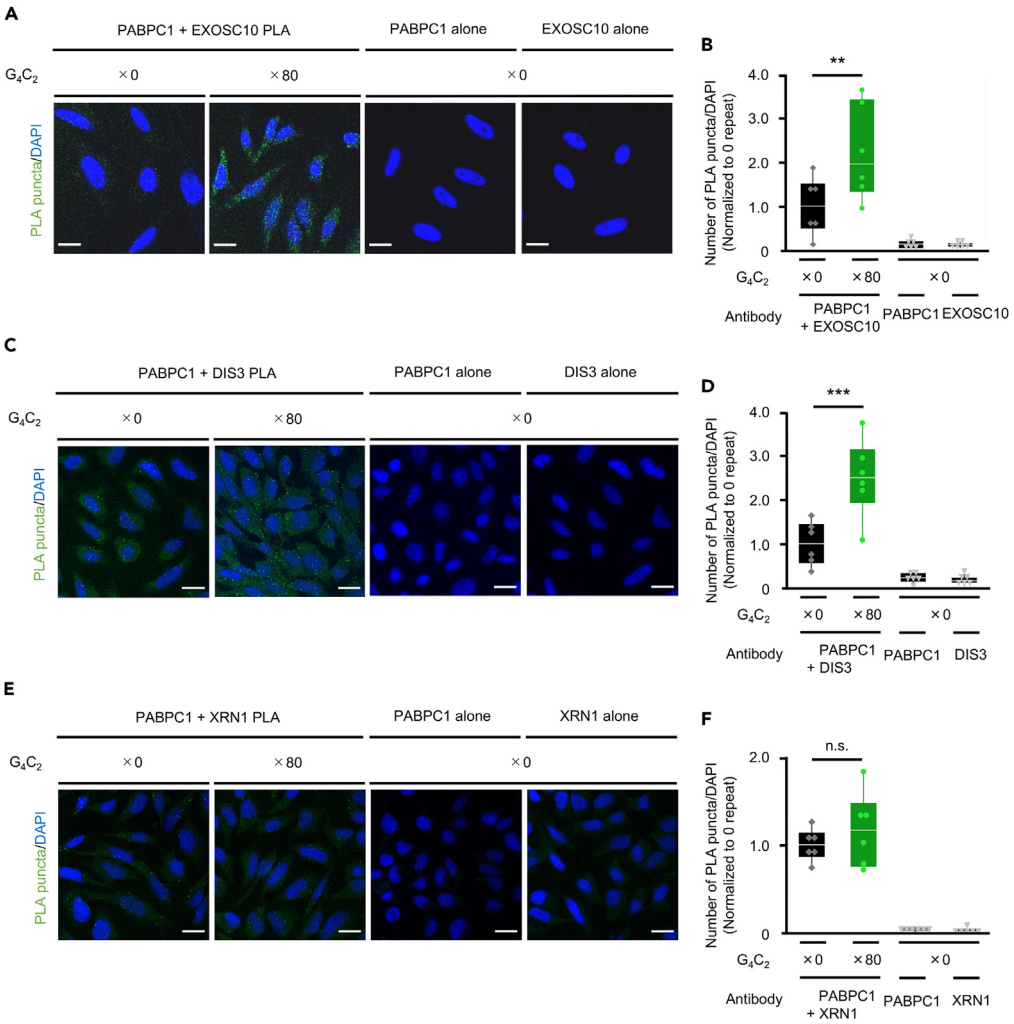

Figure 6. PABPC1 and RNA exosome complex present in proximity in G_4C_2 repeat RNA-expressing cells

(A–D) The PLA signal intensity of PABPC1 and RNA exosome components (EXOSC10 and DIS3) was increased in HeLa cells expressing the $(G_4C_2)_{80}$ repeat. (E and F) The PLA signal intensity of PABPC1 and XRN1 did not increase in HeLa cells expressing the $(G_4C_2)_{80}$ repeat compared with cells expressing the $(G_4C_2)_0$ repeat. Six independent experiments were performed. Scale bars = 20 μm **$p < 0.001$ and ***$p < 0.0001$. n.s.; not significant by two-tailed paired Student's *t*-test. A circle in the graphs represents a result of a single culture well. The center lines in the boxplots represent the median, with the 25th and 75th percentiles marked by the box limits. The whiskers represent the farthest data points. See also Figure S5.

An important consequence of RNA accumulation is increased global protein translation. The G_4C_2 repeat RNA is translated into DPR through RAN translation.[4–6,10,50,51] The neurotoxicity of DPR has been shown in multiple disease models and postulated in *C9*-FTLD/ALS patients.[52–57] We previously reported that siRNA-mediated knockdown of hnRNPA3 leads to increased DPR expression in cellular and *Drosophila* models of *C9*-FTLD/ALS.[15,16,19] In the current study, PABPC1 knockdown, as well as hnRNPA3 knockdown, increased G_4C_2 repeat RNA levels. Therefore, we examined whether reduced expression of PAPBC1 also increases DPR expression.

To do so, we transfected a CMV promoter-driven $(G_4C_2)_{80}$ repeat plasmid into HeLa cells (Figure 7A). Consistent with a previous report,[15] the knockdown of hnRNPA3 increased poly-GA expression (Figures 7B and 7C). Unexpectedly, the knockdown of PABPC1 had no effect on poly-GA expression (Figures 7B and 7C), despite increasing the accumulation of G_4C_2 repeat RNA compared to the control knockdown (Figure 4C). While PABPC1 and hnRNPA3 have similar effects on repeat RNA degradation, these seemingly opposite results on RAN translation suggest that hnRNPA3 has an additional activity that inhibits RAN translation, whereas PABPC1 does not. Therefore, we examined poly-GA expression through RAN translation under PABPC1 and hnRNPA3 double knockdown conditions. The simultaneous reduction in PABPC1 and hnRNPA3 expression had no additive effect on G_4C_2 repeat RNA accumulation (Figure 4C). However, this significantly increased poly-GA RAN translation compared to PABPC1 knockdown alone (Figures 7D and 7E).

Collectively, these results suggest that hnRNPA3, but not PABPC1, has a latent suppressive effect on RAN translation while sharing similar consequences on the degradation of G_4C_2 repeat RNA.

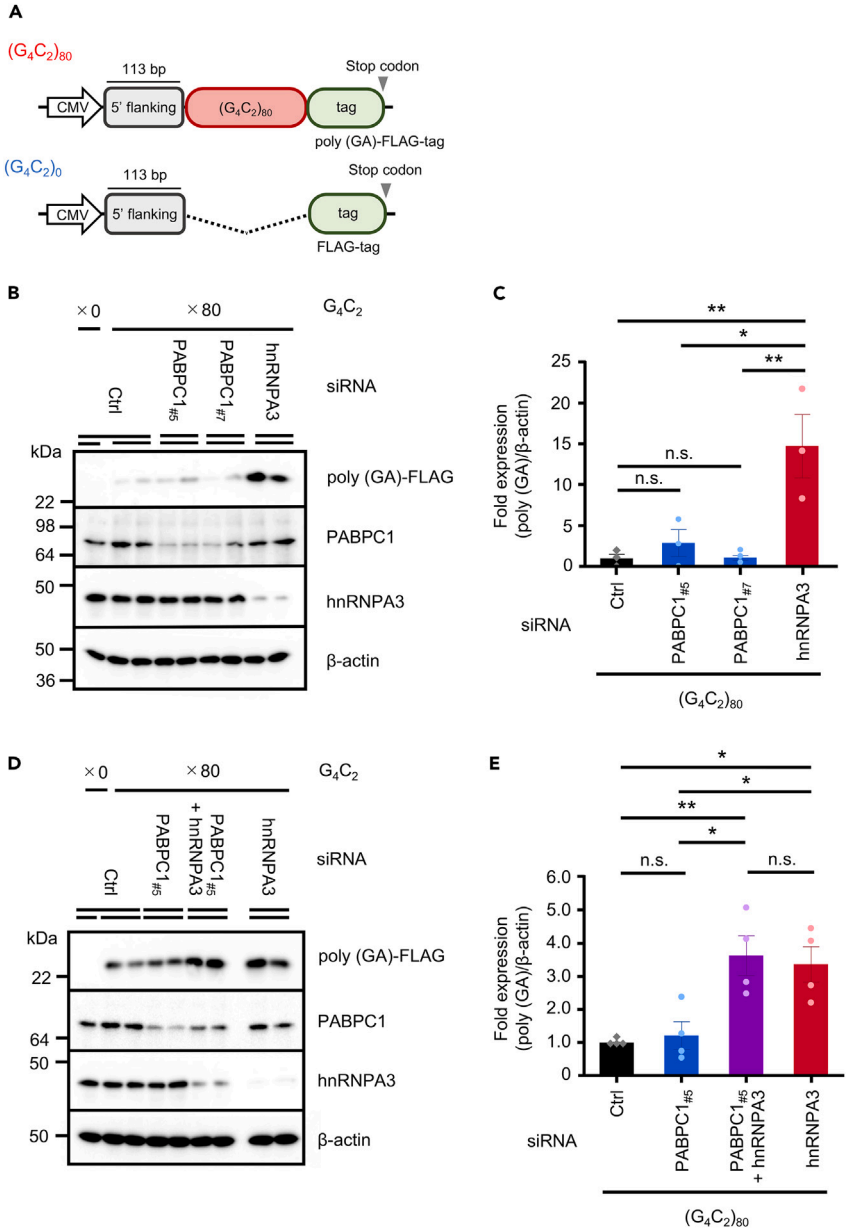

Figure 7. Simultaneous reductions of PABPC1 and hnRNPA3 promotes repeat-associated non-AUG (RAN) translation, but not when PABPC1 is reduced alone

(A) Plasmids expressing $(G_4C_2)_{80}$ repeat and $(G_4C_2)_0$ repeat. Both plasmids contained FLAG tag sequences.

(B and C) FLAG-tagged poly-GA expression increased with a single knockdown of hnRNPA3 but not with a single knockdown of PABPC1.

(D and E) FLAG-tagged poly-GA expression increased by PABPC1 and hnRNPA3 double knockdown. bp, base pair. Three (C) or four (E) independent experiments with two biological replicates were performed. A circle in the graphs represents the mean of two biological replicates. Ctrl, non-targeting siRNA; $PABPC1_{\#5}$ or $_{\#7}$, siRNA targeting PABPC1. *$p < 0.05$ and **$p < 0.001$. n.s.; not significant by one-way ANOVA with Tukey's HSD test. All bar graphs are shown as the mean ± SEM. See also Figure S6.

DISCUSSION

Because G_4C_2 repeat RNA is located upstream of *C9*-FTLD/ALS pathological cascades, it is important to elucidate the pathway of G_4C_2 repeat RNA degradation. Increased expression of hnRNPA3 reduced repeat RNA accumulation[12,15,19] and hnRNPA3 does not appear to have a direct RNA-degrading function; hence, we hypothesized that hnRNPA3 and its associating factors cooperate in the degradation of G_4C_2 repeat RNA.

Through the stringent filtering protocol followed by the secondary screening of siRNA-mediated knockdown, we revealed that some RBPs were potentially involved in *C9orf72* repeat RNA degradation in the cells. PPIA is an isoform of the peptidyl-prolyl *cis-trans* isomerase, and

DDX39B is a member of the DEAD box family of RNA-dependent ATPases. These two RBPs may indeed inhibit G_4C_2 repeat RNA degradation; however, further investigation is required for experimental validation. PABPC1[58] and hnRNPA3[12] have been reported to bind to G_4C_2 repeat RNA. The current study revealed that PABPC1 and hnRNPA3 cooperate in the G_4C_2 repeat RNA degradation pathway.

PLA signals between endogenous hnRNPA3 and endogenous PABPC1 were significantly increased in the presence of G_4C_2 repeat RNA and clear evidence of their functional interactions was provided; however, the overexpressed hnRNPA3-APEX2-mediated PABPC1 biotinylation in G_4C_2 repeat expressing cells was rather decreased. Currently, we have no clear explanation for the observation. Overexpression of hnRNPA3-APEX2 fusion construct itself might affect the intermolecular distance of hnRNPA3-APEX2 and PABPC1 in the presence or absence of G_4C_2 repeat RNA, and/or differences in detectable intramolecular distances between the two assays (<20 nm in APEX2 assay, and <40 nm in PLA) might also affect the result.

Since PABPC1 and hnRNPA3 were expected to have no intrinsic RNase activity, we assumed that there are unknown downstream effectors that collaborate with them and execute repeat RNA degradation. In this study, we suggest that the RNA exosome complex is one of such executors responsible for PABPC1-mediated G_4C_2 repeat RNA degradation. In a previous study, we showed that the RNA exosome complex is involved in G_4C_2 repeat RNA degradation.[33] In line with the evidence that G_4C_2 repeat-expanded intron-containing RNA is polyadenylated in the expansion carriers,[59] our findings implicate that PABPC1 and hnRNPA3 recognize the G_4C_2 repeat RNA transcript and recruit the RNA exosome complex, but not XRN1, to degrade the repeat RNA from the 3′ end.

Although PABPC1 predominantly localizes in the cytoplasm and interacts with the components of RNA exosome complex in the presence of G_4C_2 repeat RNA, the reduction of PABPC1 promotes the formation of RNA foci in the cell nucleus. These results suggest that in addition to its role in RNA degradation, PABPC1 may also be involved in the transport of G_4C_2 repeat RNA from the nucleus to the cytoplasm. Indeed, PABPC1 has previously been reported as a nuclear-cytoplasmic shuttling protein and is known to bind to newly synthesized RNA in the nucleus.[34,58]

PABPC1 and translation initiation factors recognize the 5′ cap and 3′ poly (A) tail of mRNA to help synthesize proteins through the AUG-dependent translation mechanism.[48,60] Since PABPC1 plays a key role in the AUG-dependent protein synthesis, we initially expected that PABPC1 may be an essential factor for RAN translation. However, this was not the case. In contrast to the reduction of hnRNPA3, the reduction of PABPC1 showed no effect on poly-GA expression levels, despite increasing G_4C_2 repeat RNA levels and RNA foci formation. Moreover, simultaneous reduction of hnRNPA3 in addition to PABPC1 unleased poly-GA expression through RAN translation. These results indicate that hnRNPA3 has an additional role in repressing RAN translation that has not previously been distinguished from its effect on repeat RNA degradation. Our current findings end up with a new question that remains to be answered; "How does hnRNPA3 inhibit RAN translation?".

Collectively, we revealed that PABPC1 in association with the RNA exosome complex plays a role in the hnRNPA3-mediated degradation of pathological G_4C_2 expanded repeat RNA. Moreover, we found a novel aspect of hnRNPA3 in the suppression of RAN translation, thus providing further evidence of the complexity between RNA degradation and translation. Our study elucidated a mechanistic example of RNA binding protein-mediated degradation of G_4C_2 repeat RNA. Facilitation of efficient degradation of G_4C_2 repeat RNA is a way to compensate neurodegeneration and may help develop new therapeutic strategy for *C9*-FTLD/ALS and even other repeat expansion diseases.

Limitations of the study

We recognize our study has at least five limitations. First, hnRNPA3-APEX2-fusion protein biotinylated proximate molecules primarily in the cytoplasm. This could be partly because the hydrophilicity of the hydroxy group attached to the phenyl group of BP makes it difficult for BP to penetrate the nuclear membrane.[26,30] Additional approaches are needed to learn about the proximity molecules of hnRNPA3 in the nucleus and the RNA degradation pathways mediated by them. Second, in the primary screening with LC-MS/MS and Gene Ontology analysis, the criteria and filtering protocols might be too stringent, and we might have missed proteins that were potentially important in the hnRNPA3-mediated G_4C_2 repeat RNA degradation pathway. Further analysis of these proteins may provide additional insights into the RNA degradation pathway, including how the silencing of PABPC1 affects RNA foci in the nucleus. Third, our study suggested that the mode of interaction between hnRNPA3 and hnRNPA3 interactors is altered by the expression of G_4C_2 repeat RNA, but whether these interactions are truly RNA-dependent has not been experimentally validated. Fourth, there is limited validation data with patient-derived cells: knockdown of PABPC1 does indeed affect the accumulation of G_4C_2 repeat RNA foci in *C9*-FTLD/ALS patient-derived fibroblasts; however, biochemical measurement of the repeat RNA and DPR levels have not been performed on patient-derived cells. Fifth, although APEX2 proteomics and PLA showed that PABPC1-hnRNPA3 and PABPC1-RNA exosome complex are in proximity in the G_4C_2 repeat RNA degradation pathway, it remains unclear the underlying molecular mechanisms by which PABPC1 interacts with hnRNPA3 and RNA exosome complex, thus leaves room for further investigations.

STAR★METHODS

Detailed methods are provided in the online version of this paper and include the following:

SUPPLEMENTAL INFORMATION

Supplemental information can be found online at https://doi.org/10.1016/j.isci.2024.109303.

ACKNOWLEDGMENTS

We thank Mr. Umihito Nakagawa and Ms. Ayako Nishioka (The Center of Medical Innovation and Translational Research, Osaka University) for LC-MS/MS analysis. We thank Editage for editing and reviewing this manuscript for the English language. The Graphical Abstract was created using BioRender.

K.M. was supported by the JSPS KAKENHI grant numbers JP20H03602, JP20H05927, and JP22K19492; JST FOREST Program under grant number JPMJFR200Z; AMED grant number 23dk0207066h0001; SENSHIN Medical Research Foundation; and Takeda Science Foundation. S.G. was supported by a JSPS Research Fellowship for Young Scientists JP22J12248. S.T. was supported by JSPS KAKENHI grant number 22K07559. M.I. was supported by AMED grant numbers JP21ek0109510h0001 and 22bm0804034h0001.

AUTHOR CONTRIBUTIONS

R.U. and K.M. designed the study. R.U. performed all experiments and analyzed all results. S.G., T.M., S.K., T.Y., Y.K., and S.A. helped design, perform, and analyze the study and experiments. K.M., S.G., S.T., and M.I. acquired funding. M.I. supervised the research. R.U. and K.M. prepared the manuscript. All authors have discussed the results and approved the final manuscript.

DECLARATION OF INTERESTS

The authors declare no competing interests.

Received: September 1, 2023
Revised: December 21, 2023
Accepted: February 16, 2024
Published: February 22, 2024

REFERENCES

1. Wen, X., Westergard, T., Pasinelli, P., and Trotti, D. (2017). Pathogenic determinants and mechanisms of ALS/FTD linked to hexanucleotide repeat expansions in the C9orf72 gene. Neurosci. Lett. *636*, 16–26. https://doi.org/10.1016/j.neulet.2016.09.007.
2. Hernandez, I., Fernandez, M.-V., Tarraga, L., Boada, M., and Ruiz, A. (2018). Frontotemporal Lobar Degeneration (FTLD): Review and Update for Clinical Neurologists. Curr. Alzheimer Res. *15*, 511–530. https://doi.org/10.2174/1567205014666170725130819.
3. Van Mossevelde, S., Engelborghs, S., van der Zee, J., and Van Broeckhoven, C. (2018). Genotype-phenotype links in frontotemporal lobar degeneration. Nat. Rev. Neurol. *14*, 363–378. https://doi.org/10.1038/s41582-018-0009-8.
4. Ash, P.E.A., Bieniek, K.F., Gendron, T.F., Caulfield, T., Lin, W.L., DeJesus-Hernandez, M., van Blitterswijk, M.M., Jansen-West, K., Paul, J.W., Rademakers, R., et al. (2013). Unconventional Translation of C9ORF72 GGGGCC Expansion Generates Insoluble Polypeptides Specific to c9FTD/ALS. Neuron *77*, 639–646. https://doi.org/10.1016/j.neuron.2013.02.004.
5. Mori, K., Weng, S.M., Arzberger, T., May, S., Rentzsch, K., Kremmer, E., Schmid, B., Kretzschmar, H.A., Cruts, M., Van Broeckhoven, C., et al. (2013). The C9orf72 GGGGCC repeat is translated into aggregating dipeptide-repeat proteins in FTLD/ALS. Science *339*, 1335–1338. https://doi.org/10.1126/science.1232927.
6. Mori, K., Arzberger, T., Grässer, F.A., Gijselinck, I., May, S., Rentzsch, K., Weng, S.M., Schludi, M.H., van der Zee, J., Cruts, M., et al. (2013). Bidirectional transcripts of the expanded C9orf72 hexanucleotide repeat are translated into aggregating dipeptide repeat proteins. Acta Neuropathol. *126*, 881–893. https://doi.org/10.1007/s00401-013-1189-3.

7. Mann, D.M.A., Rollinson, S., Robinson, A., Bennion Callister, J., Thompson, J.C., Snowden, J.S., Gendron, T., Petrucelli, L., Masuda-Suzukake, M., Hasegawa, M., et al. (2013). Dipeptide repeat proteins are present in the p62 positive inclusions in patients with frontotemporal lobar degeneration and motor neurone disease associated with expansions in C9ORF72. Acta Neuropathol. Commun. *1*, 68. https://doi.org/10.1186/2051-5960-1-68.
8. Lagier-Tourenne, C., Baughn, M., Rigo, F., Sun, S., Liu, P., Li, H.-R., Jiang, J., Watt, A.T., Chun, S., Katz, M., et al. (2013). Targeted degradation of sense and antisense C9orf72 RNA foci as therapy for ALS and frontotemporal degeneration. Proc National Acad Sci *110*, E4530–E4539. https://doi.org/10.1073/pnas.1318835110.
9. Mizielinska, S., Lashley, T., Norona, F.E., Clayton, E.L., Ridler, C.E., Fratta, P., and Isaacs, A.M. (2013). C9orf72 frontotemporal lobar degeneration is characterised by frequent neuronal sense and antisense RNA foci. Acta Neuropathol. *126*, 845–857. https://doi.org/10.1007/s00401-013-1200-z.
10. Gendron, T.F., Bieniek, K.F., Zhang, Y.-J., Jansen-West, K., Ash, P.E.A., Caulfield, T., Daughrity, L., Dunmore, J.H., Castanedes-Casey, M., Chew, J., et al. (2013). Antisense transcripts of the expanded C9ORF72 hexanucleotide repeat form nuclear RNA foci and undergo repeat-associated non-ATG translation in c9FTD/ALS. Acta Neuropathol. *126*, 829–844. https://doi.org/10.1007/s00401-013-1192-8.
11. DeJesus-Hernandez, M., Finch, N.A., Wang, X., Gendron, T.F., Bieniek, K.F., Heckman, M.G., Vasilevich, A., Murray, M.E., Rousseau, L., Weesner, R., et al. (2017). In-depth clinico-pathological examination of RNA foci in a large cohort of C9ORF72 expansion carriers. Acta Neuropathol. *134*, 255–269. https://doi.org/10.1007/s00401-017-1725-7.
12. Mori, K., Lammich, S., Mackenzie, I.R.A., Forné, I., Zilow, S., Kretzschmar, H., Edbauer, D., Janssens, J., Kleinberger, G., Cruts, M., et al. (2013). HnRNP A3 binds to GGGGCC repeats and is a constituent of p62-positive/TDP43-negative inclusions in the hippocampus of patients with C9orf72 mutations. Acta Neuropathol. *125*, 413–423. https://doi.org/10.1007/s00401-013-1088-7.
13. Bampton, A., Gittings, L.M., Fratta, P., Lashley, T., and Gatt, A. (2020). The role of hnRNPs in frontotemporal dementia and amyotrophic lateral sclerosis. Acta Neuropathol. *140*, 599–623. https://doi.org/10.1007/s00401-020-02203-0.
14. Davidson, Y.S., Flood, L., Robinson, A.C., Nihei, Y., Mori, K., Rollinson, S., Richardson, A., Benson, B.C., Jones, M., Snowden, J.S., et al. (2017). Heterogeneous ribonuclear protein A3 (hnRNP A3) is present in dipeptide repeat protein containing inclusions in Frontotemporal Lobar Degeneration and Motor Neurone disease associated with expansions in C9orf72 gene. Acta Neuropathol. Commun. *5*, 31. https://doi.org/10.1186/s40478-017-0437-5.
15. Mori, K., Nihei, Y., Arzberger, T., Zhou, Q., Mackenzie, I.R., Hermann, A., Hanisch, F.; German Consortium for Frontotemporal Lobar Degeneration, Bavarian Brain Banking Alliance, and Kamp, F., et al. (2016). Reduced hnRNPA3 increases C9orf72 repeat RNA levels and dipeptide-repeat protein deposition. EMBO Rep. *17*, 1314–1325. https://doi.org/10.15252/embr.201541724.
16. Nihei, Y., Mori, K., Werner, G., Arzberger, T., Zhou, Q., Khosravi, B., Japtok, J., Hermann, A., Sommacal, A., Weber, M., et al. (2020). Poly-glycine–alanine exacerbates C9orf72 repeat expansion-mediated DNA damage via sequestration of phosphorylated ATM and loss of nuclear hnRNPA3. Acta Neuropathol. *139*, 99–118. https://doi.org/10.1007/s00401-019-02082-0.
17. Papadopoulou, C., Boukakis, G., Ganou, V., Patrinou-Georgoula, M., and Guialis, A. (2012). Expression profile and interactions of hnRNP A3 within hnRNP/mRNP complexes in mammals. Arch. Biochem. Biophys. *523*, 151–160. https://doi.org/10.1016/j.abb.2012.04.012.
18. Martin, E.W., Holehouse, A.S., Peran, I., Farag, M., Incicco, J.J., Bremer, A., Grace, C.R., Soranno, A., Pappu, R.V., and Mittag, T. (2020). Valence and patterning of aromatic residues determine the phase behavior of prion-like domains. Science *367*, 694–699. https://doi.org/10.1126/science.aaw8653.
19. Taminato, T., Takeuchi, T., Ueyama, M., Mori, K., Ikeda, M., Mochizuki, H., and Nagai, Y. (2023). Therapeutic reduction of GGGGCC repeat RNA levels by hnRNPA3 suppresses neurodegeneration in Drosophila models of C9orf72 -linked ALS/FTD. Hum. Mol. Genet. *32*, 1673–1682. https://doi.org/10.1093/hmg/ddac298.
20. Lin, Y., Protter, D.S.W., Rosen, M.K., and Parker, R. (2015). Formation and Maturation of Phase-Separated Liquid Droplets by RNA-Binding Proteins. Mol. Cell *60*, 208–219. https://doi.org/10.1016/j.molcel.2015.08.018.
21. Nott, T.J., Petsalaki, E., Farber, P., Jervis, D., Fussner, E., Plochowietz, A., Craggs, T.D., Bazett-Jones, D.P., Pawson, T., Forman-Kay, J.D., and Baldwin, A.J. (2015). Phase Transition of a Disordered Nuage Protein Generates Environmentally Responsive Membraneless Organelles. Mol. Cell *57*, 936–947. https://doi.org/10.1016/j.molcel.2015.01.013.
22. Wolozin, B., and Ivanov, P. (2019). Stress granules and neurodegeneration. Nat. Rev. Neurosci. *20*, 649–666. https://doi.org/10.1038/s41583-019-0222-5.
23. Teixeira, D., Sheth, U., Valencia-Sanchez, M.A., Brengues, M., and Parker, R. (2005). Processing bodies require RNA for assembly and contain nontranslating mRNAs. Rna *11*, 371–382. https://doi.org/10.1261/rna.7258505.
24. Hung, V., Udeshi, N.D., Lam, S.S., Loh, K.H., Cox, K.J., Pedram, K., Carr, S.A., and Ting, A.Y. (2016). Spatially resolved proteomic mapping in living cells with the engineered peroxidase APEX2. Nat. Protoc. *11*, 456–475. https://doi.org/10.1038/nprot.2016.018.
25. Martell, J.D., Deerinck, T.J., Sancak, Y., Poulos, T.L., Mootha, V.K., Sosinsky, G.E., Ellisman, M.H., and Ting, A.Y. (2012). Engineered ascorbate peroxidase as a genetically encoded reporter for electron microscopy. Nat. Biotechnol. *30*, 1143–1148. https://doi.org/10.1038/nbt.2375.
26. Rhee, H.W., Zou, P., Udeshi, N.D., Martell, J.D., Mootha, V.K., Carr, S.A., and Ting, A.Y. (2013). Proteomic mapping of mitochondria in living cells via spatially restricted enzymatic tagging. Science *339*, 1328–1331. https://doi.org/10.1126/science.1230593.
27. Lam, S.S., Martell, J.D., Kamer, K.J., Deerinck, T.J., Ellisman, M.H., Mootha, V.K., and Ting, A.Y. (2015). Directed evolution of APEX2 for electron microscopy and proximity labeling. Nat. Methods *12*, 51–54. https://doi.org/10.1038/nmeth.3179.
28. Trinkle-Mulcahy, L. (2019). Recent Advances in Proximity-Based Labeling Methods for Interactome Mapping [version 1; referees: 2 approved]. F1000Res. *8*. https://doi.org/10.12688/f1000research.16903.1.
29. Mortensen, A., and Skibsted, L.H. (1997). Importance of Carotenoid Structure in Radical-Scavenging Reactions. J Agr Food Chem *45*, 2970–2977. https://doi.org/10.1021/jf970010s.
30. Tan, B., Peng, S., Yatim, S.M.J.M., Gunaratne, J., Hunziker, W., and Ludwig, A. (2020). An Optimized Protocol for Proximity Biotinylation in Confluent Epithelial Cell Cultures Using the Peroxidase APEX2. STAR Protoc. *1*, 100074. https://doi.org/10.1016/j.xpro.2020.100074.
31. Grant, M.K.O., Shapiro, S.L., Ashe, K.H., Liu, P., and Zahs, K.R. (2019). A Cautionary Tale: Endogenous Biotinylated Proteins and Exogenously-Introduced Protein A Cause Antibody-Independent Artefacts in Western Blot Studies of Brain-Derived Proteins. Biol. Proced. Online *21*, 6. https://doi.org/10.1186/s12575-019-0095-z.
32. Mannix, K.M., Starble, R.M., Kaufman, R.S., and Cooley, L. (2019). Proximity labeling reveals novel interactomes in live Drosophila tissue. Development *146*, dev176644. https://doi.org/10.1242/dev.176644.
33. Kawabe, Y., Mori, K., Yamashita, T., Gotoh, S., and Ikeda, M. (2020). The RNA exosome complex degrades expanded hexanucleotide repeat RNA in C9orf72 FTLD/ALS. EMBO J. *39*, e102700. https://doi.org/10.15252/embj.2019102700.
34. Hosoda, N., Lejeune, F., and Maquat, L.E. (2006). Evidence that Poly(A) Binding Protein C1 Binds Nuclear Pre-mRNA Poly(A) Tails. Mol. Cell Biol. *26*, 3085–3097. https://doi.org/10.1128/mcb.26.8.3085-3097.2006.
35. Eliseeva, I.A., Lyabin, D.N., and Ovchinnikov, L.P. (2013). Poly(A)-binding proteins: Structure, domain organization, and activity regulation. Biochemistry. *78*, 1377–1391. https://doi.org/10.1134/s0006297913130014.
36. Kedersha, N.L., Gupta, M., Li, W., Miller, I., and Anderson, P. (1999). RNA-Binding Proteins Tia-1 and Tiar Link the Phosphorylation of Eif-2α to the Assembly of Mammalian Stress Granules. J. Cell Biol. *147*, 1431–1442. https://doi.org/10.1083/jcb.147.7.1431.
37. Kedersha, N., Cho, M.R., Li, W., Yacono, P.W., Chen, S., Gilks, N., Golan, D.E., and Anderson, P. (2000). Dynamic Shuttling of Tia-1 Accompanies the Recruitment of mRNA to Mammalian Stress Granules. J. Cell Biol. *151*, 1257–1268. https://doi.org/10.1083/jcb.151.6.1257.
38. Matheny, T., Treeck, B.V., Huynh, T.N., and Parker, R. (2020). RNA partitioning into stress granules is based on the summation of multiple interactions. RNA *27*, 078204.120. https://doi.org/10.1261/rna.078204.120.
39. DeJesus-Hernandez, M., Mackenzie, I.R., Boeve, B.F., Boxer, A.L., Baker, M., Rutherford, N.J., Nicholson, A.M., Finch, N.A., Flynn, H., Adamson, J., et al. (2011). Expanded GGGGCC Hexanucleotide Repeat in Noncoding Region of C9ORF72 Causes Chromosome 9p-Linked FTD and ALS. Neuron *72*, 245–256. https://doi.org/10.1016/j.neuron.2011.09.011.
40. Ivanov, A., Mikhailova, T., Eliseev, B., Yeramala, L., Sokolova, E., Susorov, D., Shuvalov, A., Schaffitzel, C., and Alkalaeva, E.

(2016). PABP enhances release factor recruitment and stop codon recognition during translation termination. Nucleic Acids Res. *44*, 7766–7776. https://doi.org/10.1093/nar/gkw635.

41. Fifita, J.A., Zhang, K.Y., Galper, J., Williams, K.L., McCann, E.P., Hogan, A.L., Saunders, N., Bauer, D., Tarr, I.S., Pamphlett, R., et al. (2017). Genetic and Pathological Assessment of hnRNPA1, hnRNPA2/B1, and hnRNPA3 in Familial and Sporadic Amyotrophic Lateral Sclerosis. Neurodegener. Dis. *17*, 304–312. https://doi.org/10.1159/000481258.
42. Alam, M.S. (2022). Proximity Ligation Assay (PLA). In Methods in Molecular Biology (Humana Press Inc), pp. 191–201. https://doi.org/10.1007/978-1-0716-1948-3_13.
43. Fredriksson, S., Gullberg, M., Jarvius, J., Olsson, C., Pietras, K., Gústafsdóttir, S.M., Östman, A., and Landegren, U. (2002). Protein detection using proximity-dependent DNA ligation assays. Nat. Biotechnol. *20*, 473–477. https://doi.org/10.1038/nbt0502-473.
44. Meola, N., Domanski, M., Karadoulama, E., Chen, Y., Gentil, C., Pultz, D., Vitting-Seerup, K., Lykke-Andersen, S., Andersen, J.S., Sandelin, A., and Jensen, T.H. (2016). Identification of a Nuclear Exosome Decay Pathway for Processed Transcripts. Mol. Cell *64*, 520–533. https://doi.org/10.1016/j.molcel.2016.09.025.
45. LaCava, J., Houseley, J., Saveanu, C., Petfalski, E., Thompson, E., Jacquier, A., and Tollervey, D. (2005). RNA degradation by the exosome is promoted by a nuclear polyadenylation complex. Cell *121*, 713–724. https://doi.org/10.1016/j.cell.2005.04.029.
46. Puno, M.R., Weick, E.M., Das, M., and Lima, C.D. (2019). SnapShot: The RNA Exosome. Cell *179*, 282–282.e1. https://doi.org/10.1016/j.cell.2019.09.005.
47. Kilchert, C., Wittmann, S., and Vasiljeva, L. (2016). The regulation and functions of the nuclear RNA exosome complex. Nat. Rev. Mol. Cell Biol. *17*, 227–239. https://doi.org/10.1038/nrm.2015.15.
48. Wells, S.E., Hillner, P.E., Vale, R.D., and Sachs, A.B. (1998). Circularization of mRNA by Eukaryotic Translation Initiation Factors. Mol. Cell *2*, 135–140. https://doi.org/10.1016/s1097-2765(00)80122-7.
49. Schmidt, E.K., Clavarino, G., Ceppi, M., and Pierre, P. (2009). SUnSET, a nonradioactive method to monitor protein synthesis. Nat. Methods *6*, 275–277. https://doi.org/10.1038/nmeth.1314.
50. Zu, T., Liu, Y., Bañez-Coronel, M., Reid, T., Pletnikova, O., Lewis, J., Miller, T.M., Harms, M.B., Falchook, A.E., Subramony, S.H., et al. (2013). RAN proteins and RNA foci from antisense transcripts in C9ORF72 ALS and frontotemporal dementia. Proc National Acad Sci *110*, E4968–E4977. https://doi.org/10.1073/pnas.1315438110.
51. Mori, K., Gotoh, S., and Ikeda, M. (2023). Aspects of degradation and translation of the expanded C9orf72 hexanucleotide repeat RNA. J. Neurochem. *166*, 156–171. https://doi.org/10.1111/jnc.15847.
52. Tran, H., Almeida, S., Moore, J., Gendron, T.F., Chalasani, U., Lu, Y., Du, X., Nickerson, J.A., Petrucelli, L., Weng, Z., and Gao, F.B. (2015). Differential Toxicity of Nuclear RNA Foci versus Dipeptide Repeat Proteins in a Drosophila Model of C9ORF72 FTD/ALS. Neuron *87*, 1207–1214. https://doi.org/10.1016/j.neuron.2015.09.015.
53. Mizielinska, S., Grönke, S., Niccoli, T., Ridler, C.E., Clayton, E.L., Devoy, A., Moens, T., Norona, F.E., Woollacott, I.O.C., Pietrzyk, J., et al. (2014). C9orf72 repeat expansions cause neurodegeneration in Drosophila through arginine-rich proteins. Science *345*, 1192–1194. https://doi.org/10.1126/science.1256800.
54. Kwon, I., Xiang, S., Kato, M., Wu, L., Theodoropoulos, P., Wang, T., Kim, J., Yun, J., Xie, Y., and McKnight, S.L. (2014). Poly-dipeptides encoded by the C9orf72 repeats bind nucleoli, impede RNA biogenesis, and kill cells. Science *345*, 1139–1145. https://doi.org/10.1126/science.1254917.
55. Quaegebeur, A., Glaria, I., Lashley, T., and Isaacs, A.M. (2020). Soluble and insoluble dipeptide repeat protein measurements in C9orf72-frontotemporal dementia brains show regional differential solubility and correlation of poly-GR with clinical severity. Acta Neuropathol. Commun. *8*, 184. https://doi.org/10.1186/s40478-020-01036-y.
56. Saberi, S., Stauffer, J.E., Jiang, J., Garcia, S.D., Taylor, A.E., Schulte, D., Ohkubo, T., Schloffman, C.L., Maldonado, M., Baughn, M., et al. (2018). Sense-encoded poly-GR dipeptide repeat proteins correlate to neurodegeneration and uniquely co-localize with TDP-43 in dendrites of repeat-expanded C9orf72 amyotrophic lateral sclerosis. Acta Neuropathol. *135*, 459–474. https://doi.org/10.1007/s00401-017-1793-8.
57. Sakae, N., Bieniek, K.F., Zhang, Y.-J., Ross, K., Gendron, T.F., Murray, M.E., Rademakers, R., Petrucelli, L., and Dickson, D.W. (2018). Poly-GR dipeptide repeat polymers correlate with neurodegeneration and Clinicopathological subtypes in C9ORF72-related brain disease. Acta Neuropathol. Commun. *6*, 63. https://doi.org/10.1186/s40478-018-0564-7.
58. Rossi, S., Serrano, A., Gerbino, V., Giorgi, A., Di Francesco, L., Nencini, M., Bozzo, F., Schininà, M.E., Bagni, C., Cestra, G., et al. (2015). Nuclear accumulation of mRNAs underlies G4C2-repeat-induced translational repression in a cellular model of C9orf72 ALS. J. Cell Sci. *128*, 1787–1799. https://doi.org/10.1242/jcs.165332.
59. Niblock, M., Smith, B.N., Lee, Y.B., Sardone, V., Topp, S., Troakes, C., Al-Sarraj, S., Leblond, C.S., Dion, P.A., Rouleau, G.A., et al. (2016). Retention of hexanucleotide repeat-containing intron in C9orf72 mRNA: implications for the pathogenesis of ALS/FTD. Acta Neuropathol. Commun. *4*, 18. https://doi.org/10.1186/s40478-016-0289-4.
60. Sawazaki, R., Imai, S., Yokogawa, M., Hosoda, N., Hoshino, S.I., Mio, M., Mio, K., Shimada, I., and Osawa, M. (2018). Characterization of the multimeric structure of poly(A)-binding protein on a poly(A) tail. Sci. Rep. *8*, 1455. https://doi.org/10.1038/s41598-018-19659-6.
61. Akimoto, C., Volk, A.E., van Blitterswijk, M., Van den Broeck, M., Leblond, C.S., Lumbroso, S., Camu, W., Neitzel, B., Onodera, O., van Rheenen, W., et al. (2014). A blinded international study on the reliability of genetic testing for GGGGCC-repeat expansions in C9orf72 reveals marked differences in results among 14 laboratories. J. Med. Genet. *51*, 419–424. https://doi.org/10.1136/jmedgenet-2014-102360.
62. Mori, K., Gotoh, S., Yamashita, T., Uozumi, R., Kawabe, Y., Tagami, S., Kamp, F., Nuscher, B., Edbauer, D., Haass, C., et al. (2021). The porphyrin TMPyP4 inhibits elongation during the noncanonical translation of the FTLD/ALS-associated GGGGCC repeat in the C9orf72 gene. J. Biol. Chem. *297*, 101120. https://doi.org/10.1016/j.jbc.2021.101120.

STAR★METHODS

KEY RESOURCES TABLE

REAGENT or RESOURCE	SOURCE	IDENTIFIER
Antibodies		
Rabbit anti-DYKDDDDK (FLAG) tag (WB: 1:1000)	Cell Signaling Technology	Cat# 2368; RRID: AB_2217020
Mouse anti-V5 tag (WB: 1:1000, IF: 1:1000)	Abcam	Cat# ab27671; RRID: AB_471093
Rabbit anti-hnRNPA3 (WB: 1:1000, PLA 1:1000)	Abcam	Cat# ab78300; RRID: AB_2041662
Mouse anti-PABPC1 (WB: 1:1000, IF: 1:100, PLA: 1:500)	Santa Cruz Biotechnology	Cat# sc-32318; RRID: AB_628097
Mouse anti-cyclosporin A (WB: 1:200)	Santa Cruz Biotechnology	Cat# sc-134310; RRID: AB_2169131
Mouse anti-BAT1/DDX39 (WB: 1:200)	Santa Cruz Biotechnology	Cat# sc-271395; RRID: AB_10609494
Rabbit anti-EXOSC10 (WB: 1:500, PLA: 1:100)	Atlas Antibodies	Cat# HPA028484; RRID: AB_10611250
Rabbit anti-DIS3 (WB: 1:2000, PLA: 1:500)	Proteintech	Cat# 29664-1-AP; RRID: AB_2918336
Rabbit anti-β-actin (WB: 1:1000)	Cell Signaling Technology	Cat# 4970; RRID: AB_2223172
Rabbit anti-XRN1 (PLA: 1:500)	Invitogen	Cat# PA5-5711; RRID: AB_2649702
Mouse anti-puromycin (WB: 1:25000)	Merck Millipore	Cat# MABE343; RRID: AB_2566826
Goat anti-Rabbit IgG (H + L) HRP Conjugate (WB: 1:20000)	Promega	Cat# W401B
Goat anti-Mouse IgG (H + L) HRP Conjugate (WB: 1:10000)	Promega	Cat# W402B
Bacterial and virus strains		
NEB Stable Competent *E. coli* (High Efficiency)	New England BioLabs	Cat# C3040
Chemicals, peptides, and recombinant proteins		
Streptavidin-Horseradish Peroxidase (HRP) Conjugate (Far-WB: 1:5000)	Invitrogen	Cat# SA10001
AlexaFlour 488 streptavidin conjugate (IF: 1:4000)	Invitrogen	N/A
Puromycin	Nacalai Tesque	N/A
Cycloheximide	FUJIFILM Wako	N/A
NanoLINK Streptavidin Magnetic Beads	Vector Laboratories	Cat# M-1002
Biotin-Phenol	AdipoGen	Cat# CDX-B0270
Hydrogen Peroxide solution	Nacalai Tesque	Cat# 20779-65
cOmplete Protease Inhibitor	Roche	N/A
Opti-MEM	Thermo Fisher Scientific	N/A
Lipofectamine RNAiMAX	Thermo Fisher Scientific	N/A
Lipofectamine LTX	Thermo Fisher Scientific	N/A
PLUS reagent	Thermo Fisher Scientific	Cat# 11514015
I-Block Protein-Based Blocking Reagent	Invitrogen	Cat# T2015
4%-Paraformaldehyde phosphate buffer solution	Nacalai Tesque	Cat# 09154
M-MLV Reverse Transcriptase	Promega	N/A
RiboLock RNase Inhibitor	Thermo Fisher Scientific	N/A
PCR nucleotide mix	Roche	N/A
Formamide	FUJIFILM Wako	N/A
Ribonucleoside-vanadyl complex	New England BioLabs	Cat# S1402S

(*Continued on next page*)

Continued

REAGENT or RESOURCE	SOURCE	IDENTIFIER
3′-*O*-Me-m^{7}GpppG anti-reverse cap analog (ARCA)	New England BioLabs	Cat# S1411
RQ1 RNase-free DNase	Promega	Cat# M6101
E. coli Poly (A) Polymerase	New England BioLabs	Cat# M0276
RNase Inhibitor, Murine	New England BioLabs	Cat# M0314
Agarose S	FUJIFILM Wako	Cat# 312-01193
Formaldehyde Solution	FUJIFILM Wako	Cat# 061-00411
RNA ladder (0.125–6 kb)	FUJIFILM Wako	Cat# 311-06261
Critical commercial assays		
DCA assay kit	Bio-Rad Laboratories	N/A
Silver Stain MS Kit	FUJIFILM Wako	Cat# 299-58901
RNeasy MINI kit	QIAGEN	Cat# 74106
QIAshredder	QIAGEN	Cat# 79656
TURBO DNA-*free* kit	Invitrogen	Cat# AM1907
Duolink PLA Detection Reagent	Sigma-Aldrich	N/A
Duolink *In Situ* PLA Probe Anti-Rabbit PLUS probes	Sigma-Aldrich	Cat# DUO92002
Duolink *In Situ* PLA Probe Anti-Mouse MINUS probes	Sigma-Aldrich	Cat# DUO92004
HiScribe T7 high-yield RNA synthesis kit	New England BioLabs	Cat# E2040S
RNA clean and Concentrator-25 kit	Zymo Research	Cat# R1017
Experimental models: Cell lines		
HeLa cells (human)	ATCC	Cat# CCL-2
Fibroblasts (human)	Mori et al.[15]	N/A
Oligonucleotides		
ON-TARGETplus siRNA	Dharmacon	See Table S3
Oligo-(dT) 12–18 Primer	Invitrogen	Cat# 18418012
Repeat TAG Primer Forward: TCTCAAACTGG GATGCGTAC	Mori et al.[15]	N/A
Repeat TAG Primer Reverse: GTAGTCAAGC GTAGTCTGGG	Mori et al.[15]	N/A
Repeat TAG Probe:/56-FAM/TGCAGATAT/ Zen/CCAGCACAGTGGCG/3IABkFQ/	Mori et al.[15]	N/A
β-actin Primer Forward: ACAGAGCCTCGCCTTTG	IDT	N/A
β-actin Primer Reverse: CCTTGCACATGCCGGGAG	IDT	N/A
β-actin Primer Probe:/56-FAM/TCATCCATG/Zen/ GTGAGCTGGCGG/3IABkFQ/	IDT	N/A
5′ Cy-3-labeled (C_4G_2) ×4 probe	IDT	N/A
5′ cap-/3′ poly (A) tail-attached $(G_4C_2)_0$ or $(G_4C_2)_{80}$ repeat RNA	This paper	N/A
Recombinant DNA		
Plasmid: hnRNPA3-V5 tag-APEX2 expression constructs	This paper	N/A
Plasmid: EF1 promoter-driven $(G_4C_2)_0$ or $(G_4C_2)_{80}$ repeat expression vectors	Mori et al.[15]	N/A
Plasmid: CMV promoter-driven $(G_4C_2)_0$ or $(G_4C_2)_{80}$ repeat expression vectors	Mori et al.[15]	N/A

(*Continued on next page*)

Continued

REAGENT or RESOURCE	SOURCE	IDENTIFIER
Plasmid: siRNA-resistant PABPC1 constructs	This paper	N/A
Plasmid: mCherry-hnRNPA3 constructs	Mori et al.[15]	N/A
Software and algorithms		
Mascot software	http://www.matrixscience.com/	N/A
UniProt database	https://www.uniprot.org/	N/A
Scaffold software	https://www.proteomesoftware.com/	N/A
AmiGO 2 database	http://amigo.geneontology.org/amigo	N/A
PANTHER classification system 18.0	https://pantherdb.org	N/A
ZEN software	https://www.zeiss.com/microscopy/en/products/software/zeiss-zen.html	N/A
ImageJ software	https://imagej.nih.gov/ij/	N/A
Multi Gauge software	FUJIFILM	N/A
JMP Statistical software	https://www.jmp.com/en_us/home.html	N/A
Other		
SnakeSkin dialysis tube (10-kDa molecular weight cutoff)	Thermo Fisher Scientific	Cat# 68100
Amersham Imager 600 or 680	GE Healthcare	N/A
Countess 3 automated cell counter	Invitrogen	N/A
Confocal Laser Scanning Microscope LSM710	Carl Zeiss	N/A
UltiMate 3000 Nano LC systems	Thermo Fisher Scientific	N/A
Q-Exactive	Thermo Fisher Scientific	N/A
ViiA7 Real-Time PCR System	Applied Biosystems	N/A
QuantStudio 6 Pro	Applied Biosystems	N/A
WSE-5400 Printgraph Classic	ATTO	N/A

RESOURCE AVAILABILITY

Lead contact

Further information and requests for reagents may be directed to and will be fulfilled by the Lead Contact, Kohji Mori (kmori@psy.med.osaka-u.ac.jp).

Materials availability

All reagents generated in this study will be available with a completed material transfer agreement.

Data and code availability

- Data reported in this paper will be shared by the lead contact upon request.
- This paper does not report original code.
- Any additional information required to reanalyze the data reported in this paper is available from the lead contact upon request.

EXPERIMENTAL MODEL AND STUDY PARTICIPANT DETAILS

Cell culture

HeLa cells were obtained from the American Type Culture Collection and cultured in Dulbecco's Modified Eagle Medium (DMEM, Gibco) supplemented with 10% fetal bovine serum (Sigma-Aldrich) and penicillin (100 U/mL)/streptomycin (100 μg/mL) (P/S). The cell incubator maintained its temperature at 37°C and the CO_2 concentration at 5.0%. Cell confluency was measured using a Countess 3 automated cell counter (Invitrogen). HeLa cells were seeded at a density of 1.30×10^5 cells/mL for the following biological experiments.

Patient-derived fibroblasts

We used fibroblast cell lines obtained from *C9orf72* mutation ALS cases (n = 3) and healthy cases (n = 2). The cells were acquired based on informed consent following the Helsinki Convention.[15,33] Fibroblasts were cultured in DMEM supplemented with 20% fetal calf serum (FCS) and P/S. The expanded *C9orf72* repeat sequence was verified using repeat prime PCR.[61]

METHOD DETAILS

Plasmids

The EF1 promoter- or CMV promoter-driven $(G_4C_2)_{80}$ repeat expression vectors have been described previously.[5,15,33] The control vector lacking the G_4C_2 repeat sequence (0 repeat) has also been described previously.[15] To generate the hnRNPA3-V5-APEX2 expression vector, the hnRNPA3 sequence lacking the TAA stop codon was amplified from the mCherry-hnRNPA3 vector[15] and subcloned into HindIII/BamHI sites of pcDNA5/FRT/TO vector (Invitrogen). hnRNPA3, in which repetitive and higher-structure-forming sequences have been designed to minimize while conserving the primary amino acid sequence.[15] V5 tag-APEX2-cording DNA fragments were synthesized, HPLC purified (fasmac), and subcloned into BamHI sites (hnRNPA3-V5-APEX2 vector). For rescue experiments, a siRNA-resistant version of the PABPC1 construct containing several silent mutations in siRNA-targeted sequences was obtained from GenScript. The DNA sequence was confirmed by Sanger sequencing.

siRNA-mediated knockdown and plasmid transfection

The siRNAs were obtained from Dharmacon (Table S3). Ten nanomoles of each siRNA were reverse-transfected using Opti-MEM and lipofectamine RNAi Max (Thermo Fisher Science). After overnight incubation, DMEM was exchanged and 500 ng/μL of each plasmid was transfected with lipofectamine LTX and PLUS reagent (Thermo Fisher Science). DMEM was exchanged after 6 h of incubation. The cells were cultured for 24 h after plasmids transfection for following experiments.

Western blot (WB)

HeLa cells were lysed with RIPA buffer and sonicated using a Bioruptor (BM Equipment) for 10 min with cycles of 30 s on/30 s off. SDS loading buffer was added to the cell lysates and boiled at 100°C for 10 min. The samples were then separated on a 10% tris-glycine gel and transferred onto a PVDF membrane (Sigma-Aldrich). After blocking with I-Block (Applied Biosystems) in phosphate-buffered saline (PBS), the membrane was incubated in primary antibody solution overnight at 4°C. The following day, the membrane was washed with TBST and incubated in HRP-conjugated secondary antibody solution for 1 h. HRP signals were detected with ECL Western Blotting Detection Reagents (Cytiva), and images were obtained using Amersham Imager 600 or Amersham Imager 680 (GE Healthcare). The HRP signal intensity of each protein band was quantified using Multi Gauge software (version 3.0) (FUJIFILM).

Immunofluorescence

The cells cultured on glass coverslips were fixed in 4% paraformaldehyde phosphate buffer solution (Nacalai Tesque) and permeabilized with 0.2% Triton X-100. The cells were washed with PBS and blocked with 5% FCS for 30 min at room temperature. The blocking solution was then removed, replaced with primary antibody solution, and incubated overnight at room temperature. The following day, the cells were washed with PBST for 5 min and incubated in a secondary antibody solution for 60 min at room temperature. The cells were washed thrice with PBST and further washed with PBS. The cell nuclei were counterstained with 0.1 μg/mL DAPI for 20 min at room temperature and then washed three times with 0.02% Tween in PBS. Coverslips were mounted on glass slides using ProLong Diamond Antifade (Life Technologies). Fluorescence images were obtained using a Confocal Laser Scanning Microscope LSM710 (Carl Zeiss).

APEX2 time-course assay

HeLa cells were cultured in 24-well plate. Cells were incubated in DMEM medium containing 250 μM biotin-phenol (Adipogen) for 30 min at 37°C to provide substrates for the APEX2 enzyme. Next, to stimulate the APEX2 enzyme, cells were treated with 2 mM hydrogen peroxide (H_2O_2) solution (Nacalai Tesque) for indicated time (1, 2, 5, 15, and 30 min) at room temperature. After stimulation, the medium was quickly aspirated, and APEX2-mediated biotinylation was quenched by three treatments with ice-cold quenching buffer containing 500 mM Trolox (Sigma-Aldrich), 1 M sodium ascorbate (Nacalai Tesque), and 1 M sodium azide (Wako). Cells were washed with PBS and then subjected to WB.

APEX2 proximity labeling assay

HeLa cells were cultured in 10 cm dishes. hnRNPA3-V5-APEX2 expression cells were treated with 250 μM biotin-phenol (Adipogen) for 30 min at 37°C followed by 2 mM hydrogen peroxide (H_2O_2) solution (Nacalai Tesque) for 1 min at room temperature. After treatment, APEX2-mediated biotinylation was quenched with same step as described above. Cells in dishes were treated with lysis buffer containing 50 mM Tris-HCl, 500 mM NaCl, 0.2% SDS, 1 mM DTT, 10 mM sodium azide, 10 mM sodium ascorbate, 5 mM Trolox (Sigma-Aldrich), and cOmplete protease inhibitor (Roche) for 15 min on ice to lyse cells. Cells were then scraped into microtubes with cell scrapers and sonicated for 21 min with 60-s on/30-s off cycles. The cell lysate was centrifuged (21,500 × g) for 12 min at 4°C, and the collected supernatant was diluted with the same volume of 50 mM Tris-HCl. The supernatant was transferred into a SnakeSkin dialysis tube (10-kDa molecular weight cutoff, Thermo Fisher

Science) and spun overnight at 4°C with dialysis buffer (50 mM Tris-HCl, 250 mM NaCl, 0.1% SDS, 1% Triton X-100) to remove excess biotin from the samples. The dialysis buffer was replaced every hour for the first 4 h. The next day, the total protein concentration in each sample was quantified using a DC protein assay kit (Bio-RAD), and then to align the protein concentration, samples were diluted with ultra-pure water. To collect the biotin-labeled proteins, NanoLink Streptavidin Magnetic Beads (Vector) were added to each sample and agitated overnight at 4°C. The next day, the supernatant was discarded, and magnetic beads were washed with a series of four wash buffers (Buffer 1; 2% SDS. Buffer 2; 50 mM Tris-HCl, 100 mM NaCl, 0.1% deoxycholic acid, 1% Triton X-100, 1 mM EDTA. Buffer 3; 10 mM Tris-HCl, 250 mM NaCl, 0.5% deoxycholic acid, 0.5% NP-40, 1 mM EDTA. Buffer 4; 50 mM ammonium bicarbonate) at 4°C for 5 min. Next, to dissociate biotin-labeled proteins from streptavidin beads, an SDS loading buffer containing 20 mM DTT and 2 mM biotin was added to the samples and boiled for 10 min at 100°C. Samples were prepared for subsequent SDS-PAGE experiments. The gels were stained using the Silver Stain MS kit (Wako) and used as samples for mass spectrometry to visualize the proteins.

Mass spectrometry and Gene Ontology analysis

The lanes of interest were cut from the acrylamide gels and subjected to reduction, alkylation, and in-gel trypsin digestion. Peptides were injected into UltiMate 3000 Nano LC systems (Thermo Fisher Scientific), followed directly by LC-MS/MS analysis on a Q-Exactive (Thermo Fisher Scientific). Protein identification was performed using Mascot (Mascot Distriller_version 2.5 and Mascot Server_version 2.5) (Matrix Science) software and the UniProt database. Scaffold software (version Scaffold_4.4.3) (Proteome Software Inc.) was used to quantify the detected proteins. Quantitative values (QVs) corresponding to the number of identified proteins were calculated for each treatment condition using the following criteria: Protein Threshold: 99.0% minimum, Peptide Threshold: 90.0%, and two peptides minimum. The calculated QVs of detected proteins were obtained as follows.

$$Calculated\ \ QVs\ of\ \ each\ protein\ =\ (QVs\ in\ BP\text{-}treated)\ -\ (QVs\ in\ BP\text{-}non\text{-}treated)\ -\ (QVs\ in\ streptavidin\ magnetic\ beads\ only)$$

The average QVs (AQVs) were then calculated with the mean of them in triplicates.

The AmiGO 2 database (version 2.5.17) was used for GO analysis. GO enrichment analysis was performed using PANTHER classification system (version 18.0). The following annotation filters were applied to GO analysis: Organism: Homo sapiens, Aspect: molecular function, and Contributor: UniProt.

Quantitative reverse transcription (qRT)-PCR

The cells expressing $(G_4C_2)_{80}$ repeat RNA, incubated in a 12-well plate, were lysed with Buffer RLT (RNeasy MINI kit, QIAGEN). Total RNA was then purified using the RNeasy MINI kit and QIAshredder (QIAGEN). RNA preparations were treated using a TURBO DNA-*free* kit (Invitrogen). RNA samples were then equally diluted in RNase-free water, mixed with Oligo-(dT) (Invitrogen), and incubated for 5 min at 65°C. RNA was reverse transcribed with reverse transcription reaction solution containing M-MLV Reverse Transcriptase (Promega), RiboLock RNase Inhibitor (Thermo Fisher Scientific), and PCR nucleotide mix (Roche). Quantitative reverse transcription (qRT)-PCR was performed using TaqMan technology. Probes and primers were designed for the 3′ TAG region of the repeat construct, as previously reported.[33] Repeat TAG Primer 1: TCTCAAACTGGGATGCGTAC, Repeat TAG Primer 2: GTAGTCAAGCGTAGTCTGGG, Probe:/56-FAM/TGCAGATAT/Zen/CCAGCACAG TGGCG/3IABkFQ/. β-actin primer 1: ACAGAGCCTCGCCTTTG, β-actin primer 2: CCTTGCACATGCCGGGAG, Probe:/56-FAM/TCATCCA TG/Zen/GTGAGCTGGCGG/3IABkFQ/. Quantitative RT-PCR was performed using the ViiA7 Real-Time PCR System (Applied Biosystems) or QuantStudio 6 Pro (Applied Biosystems). Each biological sample was analyzed in triplicate, and the signal intensity was computed by the $\Delta\Delta C_T$ method using β-actin as the endogenous control.

Fluorescence *in situ* hybridization (FISH)

The cells cultured on glass coverslips were fixed in 4% paraformaldehyde and permeabilized with 0.2% Triton X-100, followed by washing with 2 × SSC and then incubated at 57°C for 30 min in prehybridization solution containing 40% formamide (Wako), 2 × SSC, 0.8 mg/mL tRNA (Roche), 0.8 mg/mL single strand salmon sperm DNA (Sigma-Aldrich), 0.16% BSA, 8% Dextran sulfate (Sigma-Aldrich), 1.6 mM Ribonucleoside-vanadyl complex (New England Biolabs) and 5 mM EDTA. Then the coverslips were incubated at 57°C overnight in hybridization solution containing 40% formamide (Wako), 2 × SSC, 0.8 mg/mL tRNA (Roche), 0.8 mg/mL single strand salmon sperm DNA (Sigma-Aldrich), 0.16% BSA, 8% Dextran sulfate (Sigma-Aldrich), 1.6 mM Ribonucleoside-vanadyl complex (New England Biolabs), 5 mM EDTA, 20 ng (HeLa) or 10 ng (fibroblast)/mL 5′ Cy3-labeled (C_4G_2) × 4 probe (IDT).[39] The following day, cells were washed three times for 30 min each at 57°C with 40% formamide (Wako), 0.5 × SSC, and then with 0.5 × SSC for 10 min each at room temperature. After a brief rinsing with PBS, nuclei were stained with 0.1 μg/mL DAPI for 20 min and then washed three times with 0.02% Tween in PBS for 5 min each. Glass coverslips were mounted with ProLong Diamond Antifade (Life Technologies). Fluorescence images were obtained using a Confocal Laser Scanning Microscope LSM710 (Carl Zeiss).

Proximity ligation assay (PLA)

HeLa cells cultured on glass coverslips were fixed in 4% paraformaldehyde phosphate buffer solution (Nacalai Tesque) for 15 min, washed with PBS, and permeabilized with 0.2% Triton X-100. The proximity ligation assay (PLA) was performed according to the Duolink PLA Fluorescence Protocol (Sigma-Aldrich). The cultures were incubated in Duolink Blocking Solution at 37°C for 1 h, and then the blocking solution was

removed and replaced with primary antibody solution diluted in Duolink Antibody Diluent overnight at room temperature. The coverslips were washed twice with Wash buffer A (Sigma-Aldrich) for 5 min each, then Duolink *In Situ* PLA Probe Anti-Rabbit PLUS and Duolink *In Situ* PLA Probe Anti-Mouse MINUS probes (Sigma-Aldrich) diluted in Duolink Antibody Diluent were applied, and then the coverslips were incubated in a humidified chamber for 1 h at 37°C. After washing the coverslips with wash buffer A, ligase mixed with Duolink Ligation Buffer (Sigma-Aldrich) was applied and incubated for 30 min at 37°C. Then, the coverslips were washed twice with wash buffer A, followed by the addition of amplification solution and incubation for 100 min at 37°C. The coverslips were washed twice in wash buffer B (Sigma-Aldrich) for 10 min each and then mounted with Prolong Diamond antifade (Life Technologies). Imaging was performed using a Confocal Laser Scanning Microscope LSM710 (Carl Zeiss).

RNA *in vitro* transcription and electrophoresis

The protocol of *in vitro* transcription was described in the previous report.[62] Briefly, T7 promoter-driven $(G_4C_2)_{80}$ repeat and $(G_4C_2)_0$ expression vectors were linearized with PmeI and used as templates for *in vitro* transcription assay with HiScribe T7 high-yield RNA synthesis kit (New England Biolabs). *In vitro* transcription was performed according to the manufacturer's protocol. In this step, to attach a 5′ cap to RNA, 10 mM 3′-*O*-Me-m^7GpppG anti-reverse cap analog (ARCA) (New England Biolabs) was added, and then incubated at 37°C for 3 h. To remove plasmid DNA, the reaction mixture was treated with RQ1 RNase-free DNase (Promega) at 37°C for 15 min. Next, polyadenylation of the synthesized RNA was performed in reaction solution containing 1 mM ATP (New England Biolabs), E. coli Poly (A) Polymerase (New England Biolabs), and 4,000 U/mL Murine RNase inhibitor (New England Biolabs) at 37°C for 30 min. Then, 5′ cap- and 3′ poly (A)-attached synthesized RNA was purified using RNA Clean & Concentrator-25 kit (Zymo Research). For the quality evaluation of the synthesized RNA, 1.5% Agarose-2.2 M formaldehyde gel electrophoresis was performed with RNA ladder (0.125 - 6kb) (Wako). The images of separated RNA bands were obtained using WSE-5400 Printgraph Classic (ATTO).

In vitro transcribed RNA time-dependent degradation assays

HeLa cells were seeded in 12-well plates. After two nights of incubation, DMEM was exchanged and 200 ng/μL of each *in vitro* transcribed $(G_4C_2)_{80}$ or $(G_4C_2)_0$ repeat RNA were transfected into the cells with Opti-MEM, lipofectamine LTX, and PLUS reagent (Thermo Fisher Science) (−4 h). DMEM was exchanged again to remove excess *in vitro* transcribed RNA after 4 h of incubation (0 h). Then, cells were sequentially collected at indicated each time point (0, 3, 6, and 12 h) and washed with PBS followed by frozen immediately. The cells were subjected to qRT-PCR analysis.

Puromycin incorporation assay (SUnSET assay)

HeLa cells were treated with or without 60 μM cycloheximide (CHX) (Wako) at 37°C for 30 min and then additionally treated with 10 μg/mL puromycin (Nacalai Tesque) at 37°C for 10 min. Cells were washed with PBS and then subjected to WB.

QUANTIFICATION AND STATISTICAL ANALYSIS

RNA foci formation analysis of fluorescence *in situ* hybridization

Fluorescence images were obtained using Confocal Laser Scanning Microscope LSM710 (Carl Zeiss) and analyzed with ZEN software (Carl Zeiss). For quantification of G_4C_2 repeat RNA foci, HeLa cells and fibroblast were analyzed with a 63×/1.20 W Korr M27 oil immersion objective. Tile-scanned images merged DAPI and Cy-3 were taken at 1.0 digital zoom. The number of G_4C_2 repeat RNA foci within DAPI-positive area was counted with ZEN software and ImageJ software (Java 1.6.0_2.0) (National Institutes of Health, USA).

Statistics

Statistical analysis was performed using JMP software (version 16.0.0). False-discovery rate (FDR) was obtained using PANTHER classification system (version 18.0).